Title

Immunomodulatory Nanoparticles for Modulating Arthritis Flares

Journal

ACS Nano, 18(3)

ISSN

1936-0851

Authors

Johnson, Wade T

McBride, David

Kerr, Matthew

et al.

Publication Date

2024-01-23

DOI

10.1021/acsnano.3c05298

Peer reviewed

Published in final edited form as:

ACS Nano. 2024 January 23; 18(3): 1892–1906. doi:10.1021/acsnano.3c05298.

Immunomodulatory nanoparticles for modulating arthritis flares

Wade T. Johnson[1], **David A. McBride**[1], **Matthew D. Kerr**[1], **Anders Nguyen**[2,3], **Martina Zoccheddu**[4], **Miriam Bollmann**[2,3], **Xiaofu Wei**[5], **Ryan M. Jones**[1], **Wei Wang**[5,6], **Mattias N.D. Svensson**[2,3], **Nunzio Bottini**[7,*], **Nisarg J. Shah**[1,*]

[1]Department of Nano and Chemical Engineering, University of California, San Diego, La Jolla, CA 92093, USA

[2]Department of Rheumatology and Inflammation Research, University of Gothenburg 41346, Sweden

[3]SciLifeLab, University of Gothenburg, 41346, Sweden

[4]Department of Medicine, University of California, San Diego, La Jolla, CA 92093, USA

[5]Department of Chemistry and Biochemistry, University of California, San Diego, La Jolla, CA 92093, USA

[6]Department of Cellular and Molecular Medicine, University of California, San Diego, La Jolla, CA 92093, USA

[7]Kao Autoimmunity Institute and Division of Rheumatology, Cedars-Sinai Medical Center, Los Angeles, CA 90048, USA

Abstract

Disease modifying drugs have improved the treatment for autoimmune joint disorders such as rheumatoid arthritis, but inflammatory flares are a common experience. This work reports the development and application of flare-modulating poly(lactic-co-glycolic acid)-poly(ethylene glycol)-maleimide (PLGA-PEG-MAL)-based nanoparticles conjugated with joint-relevant peptide antigens, aggrecan$_{70\text{-}84}$ and type 2 bovine collagen$_{256\text{-}270}$, *via* thiol-Michael

*Corresponding authors: Nunzio Bottini (nunzio.bottini@cshs.org) and Nisarg J. Shah (nshah@ucsd.edu).

Author contributions:
Conceptualization: WTJ, NB, NJS
Methodology: WTJ, MNDS, NB, NJS
Investigation: WTJ, DAM, MDK, AN, MZ, MB, RMJ
Validation: WTJ, DAM, MDK, MZ
Formal Analysis: WTJ, AN, MZ, MB, XW
Data Curation: WTJ
Software: DAM
Visualization: WTJ, AN, MB, XW, NB, NJS
Funding acquisition: DAM, MDK, NB, MNDS, NJS
Project administration: NB, NJS
Supervision: NB, WW, MNDS, NJS
Resources: NB, WW, MNDS, NJS
Writing – original draft: WTJ, NJS
Writing – review & editing: WTJ, MNDS, NB, NJS
All authors reviewed the data and analysis, provided input on the manuscript, and approved the submission.

Data and materials availability:
All data are available in the main text or the supplementary materials. Sequencing data in this publication have been deposited in the NCBI's Sequence Read Archive (SRA) database. RNA-Seq data are accessible through BioProject accession number PRJNA981187.

addition. Peptide-conjugated PLGA-PEG-MAL nanoparticles encapsulated calcitriol, which acted as an immunoregulatory agent, and were termed calcitriol loaded nanoparticles (CLNP). CLNP were ~200 nm in diameter with low a polydispersity index. *In vitro*, CLNP induced phenotypic changes in bone marrow derived dendritic cells (DC), reducing the expression of costimulatory molecules, major histocompatibility complex II, and proinflammatory cytokines. Bulk RNA sequencing of DC showed that CLNP enhanced expression of the inhibitory ligand-associated *Ctla4*, a gene associated with rheumatoid arthritis. *In vivo*, CLNP accumulated in the proximal lymph nodes after intramuscular injection. Administration of CLNP was not associated with systemic immune suppression of peripheral blood cells or adverse cytokine events. In the collagen induced arthritis and SKG mouse models of arthritis, CLNP reduced clinical scores, prevented bone erosion, and preserved cartilage proteoglycan as assessed by high-resolution microcomputed tomography and histomorphometry analysis. The disease protective effects were associated with increased CTLA-4 expression in joint-localized DC and $CD4^+$ T cells but without generalized suppression of T cell-dependent immune response. The results support the potential of CLNP as modulators of disease flares in autoimmune arthropathies.

Graphical Abstract

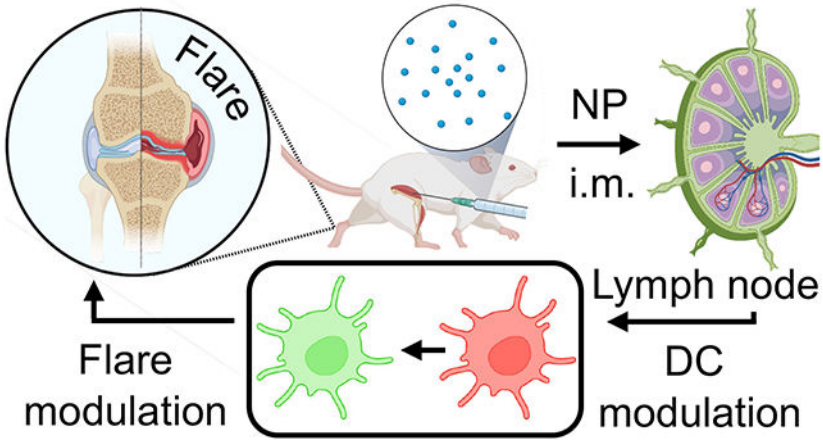

Keywords

immune engineering; rheumatoid arthritis; nanoparticles; calcitriol; flares; SKG

Chronic autoimmune joint disorders such as rheumatoid arthritis (RA) that are associated with uncontrolled joint inflammation lead to progressive destruction of articular structures, including cartilage and bone.[1,2] Disease modifying anti-rheumatic drugs (DMARD) have greatly improved treatment options. However, recurring disease fluctuations in the joints, referred to as flares, can be a common experience in otherwise adequate DMARD responders and vary in their presentation.[3-6] Current treatment focuses on symptom management with corticosteroids or non-steroidal anti-inflammatory drugs (NSAID).[7,8] However, symptomatic control is ineffective at stemming joint damage and flare recurrence.[9-11] In addition, for patients that have achieved durable disease control, tapering of the DMARD dose is appealing to reduce the risk of chronic medication. However, flares

are common when tapering is attempted.[12-14] There is an unmet need for durable flare control agents.

Although RA is a systemic disease, flares typically recur in a restricted subset of joints.[15-18] While the pathogenesis can be complex, antigen-presenting cells are key mediators, of which conventional dendritic cells (DC) are the major subset.[19-21] Preclinical mouse models have established that activated DC contribute to the development of RA pathology.[22-24] DC are thought to uptake autoantigen and/or activating stimuli in the periphery, such as from toll-like receptor (TLR) ligands and proinflammatory cytokines, and subsequently migrate to lymph nodes to prime autoreactive T cells, which have been associated with RA flares.[20,25-28] DC also infiltrate synovial tissue and fluid in response to locally produced cytokines and chemokines or differentiate locally from progenitors and are often associated with tertiary lymphoid structures.[29-35] DC in the lymph node and affected joint express classical activation markers such as major histocompatibility class 2 (MHC2), CD80/CD86, and present joint autoantigens to polarize T cells into pro-inflammatory phenotypes.[36-38] The role of DC is further supported by experiments using adoptive transfer of autoantigen-primed DC in mice, which has been shown to expand disease-specific T cells in the joint-draining lymph node.[39] On the other hand, immunomodulatory DC have been shown to impart immunoregulation through the induction of autoimmune-protective regulatory T cells (T_{reg}) and by inducing T cell anergy.[40-44] Moreover, clinical trials of adoptively transferred autologous tolerogenic DC (also generated ex vivo) have proven to be safe, without evidence of disease exacerbation or flares in humans.[45-48]

Here, we test the hypothesis that *in vivo* modulation of DC in arthritis-affected joints and proximal lymph nodes induces an arthritis flare protective effect. Our approach is based on nanoparticles (NP) delivered *via* intramuscular injection that accumulate in lymph nodes proximal to the ankle joint. We show that DC take up NP loaded with a joint antigen-relevant peptide and an immunomodulatory agent which together induce an arthritis protective effect. The NP were formulated with a biodegradable poly(lactic-co-glycolic acid)-poly(ethylene glycol) (PLGA-PEG) co-polymer functionalized with maleimide for conjugation of N-terminal cysteine peptide antigens by the thiol-Michael addition. CLNP were ~200 nm in diameter with a low polydispersity index, a size that permitted accumulation in the proximal lymph nodes.[49] CLNP encapsulated 1,25-dihydroxycholecalciferol (calcitriol), the active form of vitamin D3 known to promote an immunomodulatory DC phenotype.[50,51] Calcitriol and CLNP induced immunomodulatory bone marrow-derived DC *in vitro*, characterized by reduced expression of CD80/CD86, MHC2 and proinflammatory cytokines (IL-6 and TNF). Calcitriol and CLNP also increased CTLA-4 expression in DC. Furthermore, by bulk RNA-seq analysis, we show that calcitriol significantly alters expression of *Ctla4* and *Tgfb3* in DC, key genes associated with RA.[52,53] CLNP formulations were tested in the antigen-specific collagen induced arthritis (CIA) and the antigen-agnostic SKG model. In CIA mice, disease-specific type 2 bovine collagen$_{256\text{-}270}$ peptide (bC2)-functionalized CLNP and in SKG mice, joint relevant aggrecan$_{70\text{-}84}$ peptide (Agg)-functionalized CLNP significantly reduced clinical scores, prevented bone erosion, and reduced cartilage proteoglycan loss.

Results

Calcitriol loaded nanoparticle formulations accumulate in the proximal lymph nodes

Calcitriol loaded nanoparticles (CLNP) were formulated with poly-(lactic-co-glycolic)-polyethylene glycol-maleimide (PLGA-PEG-MAL) and calcitriol by nanoprecipitation (Fig 1a). In a subset of formulations, N-terminus modified cysteine peptides were conjugated to the PLGA-PEG-MAL (Supplementary Table 1) prior to nanoprecipitation. Post conjugation BCA analysis of the particles showed a quantitative yield of peptide bound to the polymer. To estimate the hydrodynamic diameter, unconjugated CLNP, ovalbumin peptide-conjugated CLNP (OVA-CLNP), type 2 bovine collagen peptide-conjugate CLNP (bC2-CLNP) or aggrecan peptide-conjugated CLNP (Agg-CLNP) suspended in DI water were transferred to a cuvette and analyzed using dynamic light scattering (DLS). Unconjugated CLNP had a z-avg of 96.6nm with a PDI of 0.28, OVA-CLNP had a z-avg of 233nm with a PDI of 0.10, bC2-CLNP had a z-avg of 210nm with a PDI of 0.20, and Agg-CLNP had a z-avg of 214nm with a PDI of 0.07 (Fig 1b). To measure surface charge, unconjugated CLNP, OVA-CLNP, bC2-CLNP or Agg-CLNP were suspended in DI water and transferred to a zeta potential cell. The zeta potential were as follows - unconjugated CLNP: −25.4mV, OVA-CLNP: −19.2mV, bC2-CLNP: −18.9mV and Agg-CLNP: −16.5mV (Supplementary Table 2). The aforementioned CLNP formulations were imaged using transmission electron microscopy to further characterize particle characteristics by negative stain preparation. All CLNP formulations were associated with a circular morphology. Using image analysis, the average diameters were as follows - unconjugated CLNP: 66nm ± 16nm (SD), OVA-CLNP: 160nm ± 37nm, bC2-CLNP: 129nm ± 34nm and Agg-CLNP: 128nm ± 28nm (Supplementary Fig 1).

Calcitriol release characterization was performed with ultra-high performance liquid chromatography (UHPLC) and a reverse phase column at a detection wavelength of 265 nm. UHPLC analysis showed encapsulation efficiencies (*ee*) of 9.1% for unconjugated CLNP, 10.5% for OVA-CLNP, 11.7% for bC2-CLNP, and 10.8% for Agg-CLNP. All formulations showed an initial burst release in the first three days post synthesis followed by a gradual release for at least 28 days post synthesis (Fig 1c).

To assess biodistribution *in vivo*, PLGA-PEG-MAL or calcitriol were conjugated with cyanine 5 (Cy5) and used to prepare distinct Cy5-labeled CLNP formulations. Cy5-PEG-PLGA NP were injected intramuscularly (i.m.) into the biceps femoris of C57BL/6J (B6) mice. Inguinal, popliteal, and brachial lymph nodes along with liver, kidneys and spleen were excised 2-, 8-, and 24-hours post injection and imaged on an *In Vivo* Imaging System (IVIS) (Supplementary Fig 2a). Image analysis showed that Cy5-PEG-PLGA, preferentially drained into the proximal (popliteal) lymph node (LN) at 2 hours post administration. At 8- and 24-hours post administration, the concentration of Cy5-PEG-PLGA was comparable in both the popliteal and inguinal LNs, but significantly lower, at the limit of detection, in the distal (brachial) LNs (Fig 1d). Cy5-PEG-PLGA was associated with hepatic clearance (Supplementary Fig 2b). Biodistribution of Cy5-calcitriol encapsulated in CLNP was measured following the same procedure (Supplementary Fig 2c). Image analysis showed that Cy5-calcitriol, accumulates at a similar concentration into the popliteal and inguinal

LNs at 2 hours post administration. At 8- and 24-hours post administration, Cy5-calcitrol is only detectable in the popliteal LNs (Fig 1e). Cy5-calcitriol was associated with renal clearance (Supplementary Fig 2d).

CLNP modulate dendritic cells maturation

Bone marrow derived dendritic cells (DC) were cultured *in vitro* with either free calcitriol (1nM) or CLNP (0.67μg and 6.7μg) (Fig 2a). After overnight stimulation with LPS, DC were analyzed by flow cytometry to quantify the expression of costimulatory molecules (CD80 and CD86), major histocompatibility complex 2 (MHCII) and cytotoxic T-lymphocyte-associated protein 4 (CTLA-4). DC were identified as live $CD45^{+}CD11b^{+}CD11c^{+}$ cells (Supplementary Fig 3). The 6.7μg dose of CLNP (CLNP High) reduced the fraction of $CD80^{hi+}$ DC relative to LPS treated DC (7.2%±1.4% vs 11.3%±1.5%) (Fig 2b). 1nM calcitriol, 0.67μg CLNP and 6.7μg CLNP significantly lowered the fraction of $CD86^{hi+}$ DC relative to LPS treated DC (5.7%±1.1% calcitriol, 6.5%±1.2% CLNP Low, 3.0%±0.6% CLNP High vs 13.8%±4.2% LPS control) (Fig 2c). The same groups also significantly lowered the fraction of $MHC2^{hi+}$ DC relative to LPS treated DC (2.5%±0.5% calcitriol, 3.2%±0.9% CLNP Low, 1.1%±0.2% CLNP High vs 10%±4.0% LPS control) (Fig 2d). 1nM calcitriol and 6.7μg CLNP also lowered the fraction of $MHC2^{hi+}$ DC relative to no LPS treated DC (4.5%±0.5% no LPS control). The 6.7μg dose of CLNP significantly increased the fraction of $CTLA\text{-}4^{+}$ DC relative to LPS treated DC (27%±3.9% vs 17%±3.6%) (Fig 2e).

The cell culture supernatant was analyzed for inflammatory cytokines (IL-6 and TNF) using a cytometric bead assay (CBA) kit. All treatments significantly lowered the concentration of IL-6 relative to LPS treated DC (15.8E3±0.87E3 pg/mL LPS control, 12.2E3±1.2E3 pg/mL calcitriol, 12.3E3±1.3E3 pg/mL CLNP Low, 8.2E3±1.0E3 pg/mL CLNP High) (Fig 2f). However, only the 6.7μg dose of CLNP significantly lowered the concentration of TNF relative to LPS control (16.7E3±0.30E3 pg/mL LPS control, 14.4E3±1.3E3 pg/mL CLNP High) (Fig 2g).

Calcitriol modulates disease-relevant targets in dendritic cells

The induction of an immunomodulatory DC phenotype was correlated with Next Generation RNA sequencing (RNAseq). RNAseq profiles of DC cultured in 1nM calcitriol (+ Calcitriol) or without calcitriol (− Calcitriol) were compared. Pathway enrichment analysis of the top 50 differentially expressed genes (DEG), showed significant differences in RA-associated pathway (Fig 3a). A volcano plot of RNAseq genes with those associated with RA-associated pathway highlighted in red was created; showing that *Ctla4 and Tgfb3* are the two DEG associated with RA (Fig 3b). The differential expression of *Ctla4* and *Tgfb3* was greater than 1.5-fold in + Calcitriol DC. *Ctla4* and *Tgfb3* are also visualized in a heatmap of the top 50 DEG (Fig 3c).

bC2-CLNP modulates clinical arthritis in collagen induced arthritis model

To test the concept of CLNP-mediated DC modulation *in vivo*, the collagen-induced arthritis (CIA) mouse model was used. The cysteine-modified immunodominant peptide of type 2 bovine collagen in the $I\text{-}A^{q}$ haplotype was conjugated to the PLGA-PEG-MAL and

precipitated into nanoparticles to form bC2-CLNP. DBA/1 mice were primed with an emulsion of complete Freund's adjuvant (CFA) and collagen. After 18 days, mice were treated with either free calcitriol or bC2-CLNP (33 μg bC2-CLNP or 10 ng calcitriol/day) in both biceps femoris *via* i.m. injection once a day for three days before boost with an emulsion of incomplete Freund's adjuvant (IFA) and collagen (Fig 4a). Clinical scores were monitored for 13 days post boost (Fig 4b). bC2-CLNP-treated mice presented no clinical signs of arthritis on day 6 post-boost and had scores of 6±2.6 at day 13. These scores were significantly lower than those of bolus calcitriol treated mice (1.75±0.96 & 11.5±1.3 at day 6 and day 13 respectively). Analysis of high-resolution micro-CT images (Fig 4c) of the metacarpophalangeal (Fig 4d) and ankle (Fig 4e) joints confirmed strong protection against bone erosions by bC2-CLNP as assessed by treatment-blinded bone surface area to volume ratios and bone erosion scores. In the metacarpophalangeal joint, calcitriol treated mice had an average bone surface area/volume ratio of 21.3 mm^{-1}±3.4 mm^{-1} while bC2-CLNP treated mice had an average bone surface area/volume ratio of 14.4 mm^{-1}±0.8 mm^{-1}. In the ankle joint, calcitriol treated mice had an average bone surface area/volume ratio of 27.6 mm^{-1}±2.0 mm^{-1} while bC2-CLNP treated mice had an average bone surface area/volume ratio of 17.7 mm^{-1}±5.1 mm^{-1}. Bone erosion scoring based on micro-CT scans of calcitriol treated mice averaged 2.0±1.1 and bC2-CLNP treated mice averaged 0.33±0.5, a significant difference (Fig 4f). The ankles were subsequently processed for histomorphometry and stained with hematoxylin and eosin (H&E) (Fig 5a) as well as toluidine blue (Fig 5b). Scoring of H&E-stained sections confirmed lowered synovitis (Fig 5c) and bone erosion (Fig 5d) scores in bC2-CLNP treated mice. Calcitriol treated mice had an average synovitis score of 3.75±0.46 while bC2-CLNP treated mice had an average synovitis score of 1.2±1.5. Calcitriol treated mice had an average bone erosion score of 3.13±0.64 while bC2-CLNP treated mice had an average synovitis score of 0.66±1.0. Scoring of toluidine blue-stained sections confirmed reduced proteoglycan (PG) loss scores in bC2-CLNP treated mice (Fig 5e). Calcitriol treated mice had an average PG loss score of 3.63±0.52 while bC2-CLNP treated mice had an average PG loss score of 1.33±1.37.

Agg-CLNP modulates clinical arthritis in SKG arthritis model

Unlike CIA mice, induction of arthritis in SKG mice is not associated with a specific antigen, similar to RA. Therefore, the selection of the target for immunomodulation, aggrecan, was based on abundance in the joint. The cysteine-modified immunodominant peptide of aggrecan in the I-A^d haplotype was conjugated to the PLGA-PEG-MAL and precipitated into nanoparticles to form Agg-CLNP. Agg-CLNP, OVA-CLNP, bC2-CLNP or free calcitriol were injected into each biceps femoris of SKG mice (33 μg CLNP/day or 10 ng calcitriol/day) for three days prior to arthritis flare synchronization with mannan (Fig 6a). Clinical scores were monitored for two weeks post mannan injection (Fig 6b). All groups started with clinical scores of 0. The clinical scores of Agg-CLNP treated mice were 0.23±0.091 and 0.90±0.23 at days 7 and 14 respectively, significantly lower than those of untreated mice (1.4±0.22 & 2.5±0.47), calcitriol treated mice (1.7±0.77 & 2.85±0.74), OVA-CLNP-treated mice (1.3±0.36 & 2.3±0.56), and bC2-CLNP-treated mice (0.88±0.29 & 2.5±0.47) at the same timepoints. The ankles were digested with collagenase to yield a single cell suspension before staining for $CD4^+$ T cells (Supplementary Fig 4) and innate immune cells (Supplementary Fig 5). CTLA-4^+CD4^+ T cells was significantly higher

in Agg-CLNP (47%±35%) versus untreated (2.5%±0.8%) and OVA-CLNP (3.7%±1.8%) mice (Fig 6c). CTLA-4^{+}CD11c^{+} DC were higher in Agg-CLNP (5.3%±1.1%) compared to untreated (2.8%±0.6%) and OVA-CLNP (3.2%±0.4%) mice (Fig 6d). F4-80^{+}CD11b^{+} cells were lower in the ankles of Agg-CLNP treated mice (33%±7.7%) compared to untreated mice (46%±2.8%) (Supplemental Fig 6a). Ly6G^{+} CD11b^{+} cells were higher in the ankles of Agg-CLNP treated mice (36%±3.4%) compared to untreated mice (25% ±3.2%) (Supplemental Fig 6b). qPCR analysis showed that *Tnf* was significantly lower in the ankles of Agg-CLNP treated mice (0.24±0.16) compared to untreated mice (1.0±0.33) (Fig 6e). *Il6* was lower in the ankles of Agg-CLNP treated mice (0.01±0.01) compared to untreated mice (1.4±1.4) (Fig 6f). *Mmp3* was significantly reduced in the ankles of Agg-CLNP treated mice (0.15±0.18) compared to untreated mice (1.7±0.92) (Fig 6g). *Mmp13* was significantly reduced in the ankles of Agg-CLNP treated mice (0.39±0.42) compared to untreated mice (3.9±1.3) (Fig 6h). Following the guidelines recently published for Standardized Microscopic Arthritis Scoring of Histological sections (SMASH)[54], a computer-aided algorithm in the QuPath software was generated using default settings for tissue thresholding and cell detection/classification, to facilitate quantification of cell infiltrates of H&E-stained sections (Fig 6i). Bone erosion (BE) and cartilage proteoglycan (PG) loss scoring was performed on safranin-O-stained ankle joint sections from untreated and Agg-CLNP treated mice (Fig 6j). Untreated mice ankle sections had significantly higher cell infiltrates compared to those from Agg-CLNP treated mice (Fig 6k). BE scores for untreated mouse ankles (2.0 ± 0) were significantly higher than Agg-CLNP treated mouse ankles (1.0 ± 0.7) (Fig 6l). The PG loss scores for untreated mouse ankles (1.75 ± 0.5) were significantly higher than Agg-CLNP treated mouse ankles (0.6 ± 0.5) (Fig 6m).

To measure if CLNP induced generalized immunosuppression, SKG mice were immunized against OVA by prime injection with OVA/CFA and boost injection with OVA/IFA (Supplementary Fig 7a). A subset of SKG mice received Agg-CLNP injections as previously described. Agg-CLNP treatment did not reduce anti-OVA IgG1 Ab titers in OVA immunized mice compared to untreated mice (Supplementary Fig 7b). To obtain a preliminary safety analysis, Agg-CLNP were injected into each biceps femoris of SKG mice (33 μg Agg-CLNP /day) for three days prior to arthritis flare synchronization with mannan as above. Serum was collected just before mannan injection on day 3 and blood was collected on day 7 (Supplementary Fig 8a). Blood collected on day 7 was analyzed by flow cytometry to compare peripheral blood cellular composition consisting of B cells (B220^{+}), dendritic cells (CD11c^{+}), macrophages (F4-80^{+}), neutrophils (Ly6G^{+}) and T cells (TCRβ^{+}) (Supplementary Fig 8b). There were no significant differences in the cellular composition between untreated and Agg-CLNP treated mice (Supplementary Fig 8c-g). Serum collected on day 3 was analyzed with a Th1/Th2/Th17 CBA kit to quantify proinflammatory cytokines in the peripheral blood. No significant differences in IFN-γ, IL-4, IL-6, or TNF were found between untreated and Agg-CLNP treated mice (Supplementary Fig 8h-k).

Discussion

Here, we demonstrate that joint antigen-relevant peptide-conjugated CLNP modulate arthritis flare. CLNP regulate DC maturation which, in turn, suppresses disease-specific inflammation. Phenotypic modulation of DC by CLNP was confirmed by flow cytometry

analysis and bulk next generation RNAseq, which showed a reduction in co-stimulatory CD80/CD86 expression and an increase in inhibitory CTLA-4, consistent with a tolerogenic DC phenotype. bC2-CLNP and Agg-CLNP, when administered i.m. in proximity to the joint, had potent local flare controlling effects in the CIA and SKG mouse models arthritis, respectively. Importantly, unlike standard-of-care treatment, CLNP are not immunosuppressive. Moreover, bolus systemic delivery of calcitriol had no clinical benefit in flare control supporting that both encapsulation of calcitriol and co-delivery with a disease-relevant peptide were necessary to achieve the benefit. These results support the utility of peptide conjugated CLNP as a flare control agent.

The choice of PLGA-PEG-MAL in the CLNP formulation was inspired by the long history of use of PLGA and PEG polymers in drug delivery formulations which have enabled safe and effective drug delivery.[55-58] Maleimide-cysteine conjugation has a long history and provides an efficient method to conjugate cysteine terminated peptides to maleimide functionalized polymers in mild conditions without other coupling reagents.[59,60] This method of conjugation is also utilized in multiple FDA approved antibody drug conjugates.[61-63] The immunomodulatory agent used in the formulation, calcitriol, is the active form of vitamin D3, which regulates a range of physiological processes *via* nuclear factor kappa B through the vitamin D receptor.[50] Calcitriol has also been demonstrated to mediate physiologically relevant inhibition of DC maturation and thereby modulation of antigen-specific immune responses.[51] However, calcitriol is hydrophobic with a serum half-life of ~3-6 hours.[64,65] Here, we encapsulated calcitriol in CLNP with a size ≤250 nm, which favors lymphatic drainage and is consistent with other reports.[49,55,56,66] Zeta potential measurements showed a net negative surface charge in all CLNP formulations, which is expected. Peptide conjugated formulations reduced the charge suggesting a greater localization of the peptides to the surface of the particle. UHPLC analysis determined encapsulation efficiencies ranging from 9.1% to 11.7%, and degradation studies indicated an initial burst release of calcitriol prior to a slow degradation over 28 days for an average degradation of 50% between all formulations. While this *ee* is lower compared to other reports, the formulation reported here does not use surfactants/stabilizers, which likely contributes to the encapsulation and initial degradation.[67-69] IVIS imaging of proximal and distal lymph nodes after i.m. injection of either Cy5 conjugated polymer or Cy5 conjugated calcitriol confirmed the localized biodistribution of CLNP, whereas the distal brachial LNs showed a minimal signal. Cy5-calcitriol CLNP showed a consistently strong signal in the popliteal LNs. The results indicate that CLNP readily enters the lymphatic system and is up taken within the local LN, rather than recirculating throughout the lymphatic system. IVIS analysis of the liver, kidney and spleen showed that PEG-PLGA undergoes hepatic clearance while calcitriol undergoes renal clearance, consistent with previous reports.[70]

It is well-established that calcitriol promotes an immunomodulatory DC phenotype *in vitro*, which favors induction of regulatory T cells (T_{reg}).[71-73] The tolerogenic DC phenotype is characterized by lower costimulatory molecule expression (CD80 and CD86) as well as lowered proinflammatory cytokine expression. Our *in vitro* studies clearly show that both free calcitriol and CLNP impart the tolerogenic phenotype on DC as measured by lower CD80, CD86, MHC2, IL-6 and TNF expression relative to LPS only stimulated control.

In our studies, RNAseq of *in vitro* DC cultured with calcitriol confirmed that *Ctla4* was one of the most prominent differentially expressed genes, and flow cytometry analysis of DC treated with CLNP confirmed a significant increase in CTLA-4 expression. While CTLA-4 is generally associated with T cells,[74] CTLA-4 expression in DC has been shown to influence cell function and antigen presentation, resulting in a regulatory role.[75,76] KEGG pathway enrichment analysis showed that calcitriol significantly affects the rheumatoid arthritis pathway in DC. Of the genes associated with this pathway, *Ctla4* and *Tgfb3* were significantly upregulated in calcitriol-treated DC. *Ctla4* is a known risk factor in RA and TGFβ3 has been shown to promote cartilage repair in the presence of synovial fluid from RA patients.[77,78]

Unlike autoimmune disorders where the predominant autoantigen is known, the identification of antigenic targets in RA is challenging as the complex pathology is not well-defined. RA involves a combination of genetic, environmental, and stochastic factors, and it is likely that multiple antigens are involved in disease initiation and progression. To this end, targeting multiple antigens utilizing an ex-vivo tolerogenic DC has been demonstrated.[46] In this work, the selection of the peptide for CLNP treatment in the CIA model was based on the known I-$A^{(q)}$ restricted peptide sequence for bovine collagen II (bC2).[79] On the other hand, the lack of a well-defined autoantigen target in SKG mice, emulated human RA. Inspired by the results from the proteoglycan-induced inflammatory arthritis (PGIA) model[80], we selected aggrecan, a cartilage-specific proteoglycan core protein that is enriched in the joint, with the goal of avoiding systemic exposure. As the SKG mice used were on the BALB/c background, a strain that is susceptible to PGIA, we utilized the known immunodominant peptide of aggrecan for the I-$A^{(d)}$ haplotype.[81] As controls, we used the I-$A^{(b)}$ restricted immunodominant peptide of ovalbumin and the I-$(A)^{q}$ restricted immunodominant peptide of bC2, in the SKG mice.

CLNP treatment reduced flaring in both the CIA and SKG mouse models of RA. Here, the study was designed to initially induce pathogenic collagen-specific T cells by the priming with bC2 emulsified in CFA and resembles pre-RA. Before boost, which rapidly increases joint inflammation, mice were treated with bC2-CLNP. Unlike the CIA mice, SKG mice are predisposed to inflammatory arthritis due to a mutation in *Zap70* of the T cell receptor. The use of mannan, a fungal component, synchronizes arthritis and resembles a flare. By injecting CLNP prior to mannan injection, we assessed the flare prevention effect of CLNP. Our observation was that the anti-flare effects were more pronounced in CIA compared to SKG mice, which we attribute to the use of a peptide that is derived from bC2, which also induces the disease. In both models, the use of relevant peptide CLNP reduced inflammation relative to untreated, bolus calcitriol, or irrelevant peptide CLNP formulations. Flow cytometry analysis of ankles from SKG mice showed a significant increase in CTLA-4 expression on T cells, supporting our hypothesis that CLNP modulate DC in the lymph nodes which, in turn, have a down-stream effect on T cells. Joint-localized DC also upregulated CTLA-4, consistent with the RNA-seq and *in vitro* DC culture observations. The inflammatory markers *Il6* and *Tnf* and transcripts of the joint destructive matrix metalloproteinases (MMP) *Mmp3* and *Mmp13* were reduced in the joints of mice that received Agg-CLNP.[82-84] These results support the utility of encapsulation of calcitriol and the use of disease relevant peptides in order to achieve clinical and immunological

effects. Agg-CLNP were assessed to have an acceptable safety profile, assessed by a lack of peripheral blood cytopenia and lack of upregulation of inflammatory cytokines in SKG mice. The comparable anti-OVA antibody titers in Agg-CLNP treated mice and untreated OVA immunized mice show that the results are not due to generalized immunosuppression. This is a key distinction from the current standard of care of corticosteroid injections for treatment of arthritis flares.

In the clinic, current flare treatment focuses on symptomatic management with corticosteroids (oral, intramuscular, intra-articular) or oral NSAIDs.[85] However, these medications are not joint protective, do not reduce flare recurrence and their chronic use is associated with significant side-effects. Moreover, as ~80% of flares are short-lived (< 3 days)[7], switching DMARDs to treat flares is not indicated for most patients due to the inherent risks of drug intolerance and inadequate responsiveness. CLNP are well-positioned to supplement these first-line symptomatic treatments and could also be combined with standard second-line treatment DMARDs to prevent flaring in patients with RA in remission. Other drug development programs are focused on the concept of immunomodulation through DC. For example, ex vivo generated tolerogenic DC have been shown to reduce arthritis in rodent models of RA.[86,87] Adoptively transferred autologous tolerogenic DC (also generated ex vivo) have proven to be safe in humans, without evidence of disease exacerbation or flares.[46] However, despite infusion of high doses of DC (up to ~10^7 cells), clinical benefit against RA progression or flares has remained elusive. Moreover, the complexity in the manufacturing of DC therapies presents a challenge to its widespread adoption. On the other hand, CLNP modulation of DC compares favorably to DC therapy. The general approach of using antigen-specific immunomodulatory nanoparticles has been recently tested in clinical trials for RA which has demonstrated initial positive results.[88] CLNP may serve as an immunoregulatory adjuvant to treat patients that experience recurrent local flares, potentially in combination with DMARDs without generalized immunosuppressive side effects.

Methods

Study design

The objective of this study was to develop an immunomodulatory agent to facilitate inflammation control during an arthritis flare. To this end, we formulated and characterized CLNP formulations. We validated the nanoprecipitation method to generate CLNP by synthesizing three initial lots for characterization by DLS. All material characterization studies (DLS, Zeta, TEM, and UHPLC) were conducted in triplicate with all formulations. All cell culture studies were performed with a minimum of three technical replicates. Three technical replicates were used for RNA-Seq analysis. For *in vivo* studies, outcomes were determined by assessing clinical scores, ankle thickness, flow cytometry assessments and histological appearances, unless otherwise noted. For SKG arthritis studies, littermate mice were injected with mannan to synchronize disease onset. The criteria for omission were (i) signs of arthritis on day 0 and (ii) failure to develop arthritis by day 17. All other animals were included in the data analysis. Endpoints for data collection were based on changes in and progression of clinical scores in the treatment groups. For CIA arthritis

studies, littermate mice were injected with bC2/CFA on day 0 and bC2/IFA on day 21 to synchronize disease onset. The criteria for omission were (i) signs of arthritis on day 21 and (ii) failure to develop arthritis by day 34. All other animals were included in the data analysis. Endpoints for data collection were based on changes in and progression of clinical scores in the treatment groups. Sample size for each individual experiment is provided in the figure legends. To achieve adequate power, all mouse arthritis studies were conducted by combining at least two age-matched litters. In general, statistical power for arthritis studies was based on prior reports of and our experience with arthritis mouse models.

Materials

Poly (lactide-co-glycolide)-polyethylene glycol-maleimide (50:50 L:G 20 kD PLGA, 2kD PEG SKU: 2794-20K-2000-1g, lots: 2794200202 & 2794200203) was purchased from NanoSoft polymers. Cy5-polyethylene glycol-thiol (2kD, FL078003-2K, lot: 20201217BL05,) was purchased from Biochempeg. Calcitriol (71820, lots: 0601887-33, 0601887-38, 0601887-53, 0601887-69) was purchased from Cayman Chemical. Dimethyl sulfoxide (DMSO, D128-500, lot:194474) and acetonitrile (A998-1, lot: 206498) were purchased from Fischer Chemical. 400 mesh copper grids with lacey carbon support (01824, lot: 160223) were purchased from Ted Pella. NanoW™ negative stain (2018-5ML, lot: 09S662) was purchased from Nanoprobes. Mannan (M7504-5G, lot: SLCF4977), lipopolysaccharide (LPS, L3012-5MG, lot: 0000091258), type VIII collagenase (C2139-1G, lot: 0000194156), DNase I (10104159001, lot: 60852700) and fetal bovine serum (FBS, F2442-500ML, 20K286) were purchased from Sigma-Aldrich. RPMI powder (31800-022, lot: 2338416) was purchased from Gibco. Incomplete Freund's Adjuvant + Ovalbumin (EK-0311, lots: 111, 115, 125), Complete Freund's Adjuvant + Ovalbumin (EK-0301, lots: 111, 115, 125), Incomplete Freund's Adjuvant + bovine collagen (EK-0221, lot: 102), Complete Freund's Adjuvant + bovine collagen (EK-0220, lot: 101) were purchased from Hooke Labs. Cy5-acid (BP-22274, lot: CY5-1G-1) was purchased from BroadPharm. 4-dimethylaminopyridine (148270250, lot: A0386855) was purchased from Acros Organics. N, N′-Dicyclohexylcarbodiimide (DCC, A10973, lot: 10209304) was purchased from Alfa Aesar. Dialysis sacs (12kD, D6191-25EA) were purchased from Millipore Sigma. 70 μm cell strainers (22-363-548, lot: 2021115) and 6-well culture plates (353046) were purchased from Fisher. GM-CSF (315-03-250UG, lot: 081955 L0821) was purchased from Peprotech. 96-well high affinity ELISA plates (3590) were purchased from Corning. Biotin anti-mouse IgG1 (406604, lot: B270354) was purchased from Biolegend. EDTA coated microtubes (365974, lot: 2181885), Mouse Inflammation CBA kit (552364, lot: 316578), and Mouse Th1/Th2/Th17 CBA kit (560485, lot: 3164034) were purchased from BD. Ovalbumin (OVA, vac-stova, lot: 5823-43-01) was purchased from Invivogen.

Mouse models

All animal work was approved by the UCSD Institutional Animal Care and Use Committee (IACUC) under protocol # S17160 and followed the National Institutes of Health guidelines and relevant AALAC-approved procedures. C57BL/6J (B6, Jax #000664) and DBA/1JBomTac (DBA-1, Taconic Labs #DBA1BO-M) were purchased, BALB/c SKG mice were obtained through a Materials Transfer Agreement between UC San Diego and Kyoto

University and colonies were maintained at UCSD. BALB/c SKG mice used were both male and female. In each study, mice used were either all males or all females.

Arthritis in SKG mice was synchronized in 8–12-week-old SKG mice *via* intraperitoneal (i.p.) injection of 20 mg mannan dissolved in 200 μL of sterile PBS. Disease severity was determined twice weekly using clinical scoring and measurement of hind paw swelling using calipers while mice were anesthetized. Fore and hind paws were assessed independently in each mouse and were assigned scores according to the following criterion: no visible swelling (0), mild to moderate swelling (0.5), severely swollen (1.0), as well as an additional for 0.1 for each swollen digit. Clinical scores reported are the aggregate of all paws (maximum of 5.8) from a single mouse unless otherwise noted. A score of 5.5 was considered the clinical endpoint and mice who attained this score before the end of the study were sacrificed according to IACUC guidelines.

Collagen induced arthritis (CIA) was induced in 8-week-old male DBA-1 mice by a prime injection of 50 μL bovine collagen/CFA emulsion subcutaneously in the tail on day 0 and a boost injection of 50 μL bovine collagen/IFA emulsion subcutaneously in the tail on day 21. After boost, mice were clinically scored 3x/week. Clinical scoring was performed for each limb (both wrists and both ankles) and each limb received a score of 0-4 as follows: no visible swelling/redness (0), mild but definite redness and swelling of the ankle or wrist, or apparent redness and swelling limited to individual digits, regardless of the number of affected digits (1), moderate redness and swelling of ankle or wrist (2), severe redness and swelling of the entire paw including digits (3), maximally inflamed limb with involvement of multiple joints (4). Clinical scores reported are the aggregate of all paws (maximum of 16) from a single mouse unless otherwise noted. A score of 16 was considered the clinical endpoint and mice who attained this score before the end of the study were sacrificed.

Calcitriol loaded nanoparticle (CLNP) synthesis

Cysteine-terminated peptides (Peptide 2.0) were added in a 1:1 molar ratio to 20 mg of PLGA-PEG-MAL and dissolved in 1 mL of DMSO. This mixture was agitated overnight. 60 μL of 1 mg/mL calcitriol in DMSO was then added to the polymer solution. The polymer solution was then added dropwise to 30 mL of stirring MilliQ water and stirred for 1 hour. The nanoparticle solution was then transferred to a 12 kD dialysis bag and placed in a 6 L water bath. The water bath solution was changed every 3 hours for a total 9-hour dialysis against 18 L of water. The nanoparticle solution was then stored in a 50 mL conical vial at 4°C until further use. Fresh nanoparticle solutions were prepared for each study.

CLNP characterization

An aliquot of undiluted nanoparticles was added to a cuvette and placed in a Malvern Zetasizer Pro for dynamic light scattering analysis. An aliquot of undiluted nanoparticles was added to a zeta potential cell and placed in a Malvern Zetasizer Pro for zeta potential analysis. Measurements with the Zetasizer Pro utilize ZS XPLORER software. Encapsulation of calcitriol in CLNP was determined on an UltiMate 3000 UHPLC (ThermoFischer Scientific). Briefly, nanoparticle suspensions were spun down at 21100g for 10 minutes in a centrifuge. The supernatant was aspirated, and the pellet dissolved in

HPLC grade acetonitrile. The solutions were run in a Ascentis® Express 90Å C18 reverse phase column (MilliporeSigma, Cat#53825-U, lot: USWM003951) with a mobile phase of 100% acetonitrile at an isocratic flow rate of 0.1 mL/min. Area under the curve values were compared to a standard plot of known calcitriol concentrations run in the same conditions. The encapsulation efficiency (*ee*) of calcitriol in the formulations was calculated using the following equation:

$$ee(\%) = \frac{\textbf{Calcitriol concentration in particle}}{\textbf{Calcitriol concentration in reaction}} \times \mathbf{100}$$

TEM imaging of nanoparticles was performed on a ThermoFisher Talos 200 TEM. Briefly, 2 μL of the formulation was placed on the lacey carbon side of a copper grid (Ted Pella, PN: 01824) and allowed to air dry. A drop of 2% organic tungsten stain (NanoProbes, PN: 2018-5ML) was placed on the grid, and excess was wicked away with a kimwipe. A second drop of negative stain was added and excess was wicked away with a kimwipe. The grids were allowed to air dry for 48 hours before imaging. Size measurements were performed with ImageJ software.

In vitro dendritic cell differentiation assay

B6 mouse bone marrow cells were harvested by homogenizing the long bones using a mortar and pestle in complete 1640 RPMI media with 10% FBS and 20 ng/mL GM-CSF. The homogenate was strained through a 70 μm cell strainer. The strained solution was diluted to 2,000,000 cells/mL with media and 2 mL were added per well to a tissue culture treated 6-well plate. In a subset of wells, calcitriol and/or nanoparticles were added at the concentrations as described in the results. Plates were incubated at 37°C at 5% CO_2. On day 3 of the culture, the wells were supplemented with 2 mL of fresh complete 1640 RPMI media containing GM-CSF and fresh calcitriol/CLNP to maintain experimental concentrations. On day 6 of the culture, half of the media was carefully removed and 2 mL of fresh media and fresh calcitriol/CLNP were added to maintain experimental concentrations. LPS was added at 50 ng/mL LPS for DC activation. After overnight activation, DC were analyzed by flow cytometry.

Cytometric bead assay (CBA)

Mouse inflammation CBA kit or Th1/Th2/Th17 CBA kit were purchased from BD and the assay performed according to the manufacturer's protocol. Briefly, either 50μL of cell culture supernatant or serum was added to a mixture of antibody capture beads. The beads and sample were allowed to incubate with a PE-detection reagent for two hours at room temperature. Beads were washed with buffer by centrifugation. Samples were then run on a flow cytometer and compared to a standard curve to determine cytokine concentrations.

RNA-seq of dendritic cells

DC were cultured as described above with SKG bone marrow. 1 nM calcitriol was added to a subset of DC. On day 7 of the culture, after overnight activation with LPS, the cells were transferred to a 15 mL conical tube. The cells were then sorted on a Sony SH800S cell sorter for AnnexinV^-CD11c^+ cells to isolate live DC. DC were spun down at 400 g for 5

minutes at 4°C to pellet the cells. Supernatant was removed and the cell pellets were flash frozen in liquid nitrogen before storage at −80°C. RNA was isolated and purified with a NEBNext®Ultra II Directional RNA Library Prep Kit for Illumina®, followed by 12 cycles of amplification. Sequencing was performed on an Illumina® MiSeq at the La Jolla Institute for Immunology. Data was analyzed by quantile and TMM normalization in R.

Analysis of RNA-seq

Analysis of raw reads from sequencing of RNA-seq prepared libraries went as follows: FASTQ files were aligned to mm10 reference genome using STAR with parameters "–genomeDir mm10index_fp –readFilesIn input_files –readFilesCommand gunzip -c –outFileNamePrefix bamfile_out –outSAMtype BAM SortedByCoordinate". Duplicate reads were removed using MarkDuplicates from Picard tools. Quantification through counting aligned sequencing reads counting reads within features using High-throughput sequence (HTSeq) with parameters '-f bam -r pos -s no -i gene_id -m intersection-nonempty'. Count normalization and differential RNA-seq analysis were then performed using quantile normalization and geTMM normalization after removing non-expressed genes. Differentially expressed genes (DEG) were filtered using p-values <= 0.05 and log2 fold-change >=1.5. KEGG enrichment to identify known pathways was performed using library clusterProfiler in R.

Ovalbumin immunization

On day 0, two distinct 50 μL subcutaneous injections of OVA/CFA emulsion were administered in the back of the mouse. On day 10, received a subcutaneous booster immunization of 100 μL of OVA/IFA emulsion in the back. On day 21, mice were bled by the tail vein before sacrifice. A subset of mice received 33 μg/day Agg-CLNP on days 7-9 intramuscularly in the thigh. All blood was collected into EDTA coated tubes.

Anti-OVA IgG1 antibody titer assay

Anti-OVA IgG1 antibody titers were quantified using ELISA following established protocol. High-binding ELISA plates were coated with 1 μg/mL OVA in PBS at 4 °C overnight. Blood samples were diluted ranging from 1:3 to 1:65535 and incubated with the plates at room temperature for 1.5 hours before staining for biotinylated anti-mouse IgG1. Streptavidin HRP was then incubated in the wells and subsequently developed to produce a colorimetric gradient. The anti-OVA titer was defined as the serum dilution with an optical density value closest to 0.3.

Arthritis treatment with CLNP

To assess the efficacy of CLNP in SKG arthritis, 33 μg/day of NP formulation (OVA-, bC2-, or Agg-CLNP) or bolus calcitriol (10ng/day) were injected into each biceps femoris of littermate SKG mice for 3 days prior to i.p. mannan injection on day 3. Clinical scores and ankle thickness of mice were tracked biweekly for two weeks to an endpoint on day 17. Endpoint immunological analysis of ankles was conducted with flow cytometry. In a replicate experiment, ankles were harvested for histological analysis.

To assess the efficacy of bC2-CLNP in CIA arthritis, 33 μg/day of bC2-CLNP formulation were injected into each biceps femoris of DBA-1 mice for 3 days prior to bovine collagen/IFA injection on day 21. A separate cohort of mice were treated with 10ng/day of calcitriol. Mice were clinically scored for two weeks until sacrifice on day 35. Ankles were harvested for micro-CT and histological analysis.

In vivo biodistribution

To assess the biodistribution of the polymer and the encapsulation calcitriol, both were conjugated with Cy5. PLGA-PEG-MAL and thiol-PEG-Cy5 were dissolved in a 1:1 molar ratio in DMSO (20 mg of PLGA-PEG-MAL was used) and allowed to react overnight protected from light. The nanoparticle synthesis and dialysis purification were performed with the Cy5 conjugated material as described above. To conjugate Cy5 to calcitriol, Cy5 acid (1.4 mg, 2.7 μmol), calcitriol (1 mg, 2.4 μmol) and 4-dimethylaminopyridine (0.3 mg, 2.4 μmol) in 0.3 mL of DCM were added to DCC (0.6 mg, 2.9 μmol). The mixture was allowed to mix at room temperature overnight before evaporating the solvent under a stream of air. The crude mixture was dissolved in 1 mL of DMSO and encapsulated in PLGA-PEG-MAL as described above.

In B6 mice, 33 μg/bicep femoris of either Cy5-conjugated polymer NPs, or Cy5-calcitriol encapsulated NPs were injected. Mice were sacrificed at 2, 8 and 24 hours post injection. Inguinal lymph nodes (LN), popliteal LN, brachial LN, liver, kidneys, and spleen were harvested and organized on a plastic sheet for fluorescence quantification. Fluorescent images were taken with an *In Vivo* Imaging system (Xenogen). The normalized radiant efficiency was quantified and plotted over time per organ.

Histological processing

After sacrifice, mouse hind limbs were excised below the knee joint. Muscle and skin were removed to the highest degree possible without damaging internal structures, and the limbs were fixed in 4% paraformaldehyde (PFA) for 48 hours. The fixed limbs were then transferred to a 70% ethanol solution. Samples were then sent to the University of Gothenburg (histology in Figure 5), or Inotiv (histology in Figure 6), where they were decalcified and embedded in paraffin. Paraffin embedded limbs were sectioned to an appropriate depth according to SMASH guidelines[54] and stained with hematoxylin and eosin, toluidine blue or safranin-O using standard tissue processing techniques. Stained slides were digitized using an Aperio AT2 Automated Digital Whole Slide Scanner or a Zeiss Axioscan 7 Slide Scanner.

Histomorphometry analysis

To quantify immune cell infiltration in histological sections, H&E sections were loaded into the QuPath software. Representative histological sections were used to train the software using built-in classification tools to broadly classify immune cells, muscle and tendon, and bone. Once trained, the software was then used to detect and classify types in sections from the metatarsals to part way up the tibia. Skin was excluded from the analysis to prevent misidentification of dermal cells as immune cells. For proteoglycan loss scoring and bone erosion scoring, SMASH guidelines were followed. Briefly, histological sections

were examined and proteoglycan loss was scored as follows: 0 – healthy intact cartilage consisting of fully stained cartilage layer with a smooth surface; 1 – Mild loss of staining in ~ 1/3 of the superficial cartilage zone, still predominantly red when stained with Safranin O or blue with toluidine blue; 2 – Moderate loss of Safranin O/toluidine blue staining in up to 2/3 of the superficial cartilage zone; 3 – Complete loss of Safranin O/toluidine blue staining in the superficial cartilage zone. Bone erosion was scored as follows: 0 – Healthy, intact bone surface; 1 – Small, superficial bone erosion at the outer surface of the bone, no breakage into marrow; 2 – Enhanced local bone erosions into subchondral space, partial or complete penetration of cortical bone; 3 – Massive enlarged subchondral bone erosion, extended synovial pannus invasion causing near-complete breakthrough of cortical bone to the marrow. Scoring was performed by two independent treatment-blinded operators.

Micro–computed tomography (micro-CT) analysis

Mouse ankles were placed in 4% PFA for 48 hours for fixation. After fixation, samples were transferred to 70% ethanol. Treatment-blinded scanning and analysis was performed at the University of Gothenburg. Before scanning, bones were transferred to PBS for 24 hours. Scanning was performed on a Skyscan1176 micro-CT (Bruker) with a voxel size of 9 μm, at 55 kV/467 mA, with a 0.2-mm aluminum filter. Exposure time was 880 ms. The x-ray projections were obtained at 0.4° intervals with a scanning angular rotation of 180° and a combination of four average frames. The projection images were reconstructed into three-dimensional images using Nrecon software (version 1.6.9.8, Bruker) and aligned for further analysis in DataViewer (version 1.5.0.9, Bruker). Data were processed using CT-Analyzer software (version 1.14.4.1 Bruker), and images were generated using CTVox software (version 2.7, Bruker). Bone erosion was quantified as previously described.

qPCR preparation and analysis

Agg-CLNP were administered to SKG mice prior to mannan injection as described above. Ankles were harvested 14 days after mannan injection and were flash frozen in liquid nitrogen and stored. Whole mouse joint samples were first cut and homogenized with a handheld homogenizer in TRIzol on ice (PN:15596018 Invitrogen). RNA was purified from the chloroform phase using RNAeasy Plus Micro kit (PN:74034 Qiagen) according to manufacturer's protocols. Sample RNA concentration was normalized, and cDNA was synthesized using the SuperScript III First-Strand Synthesis SuperMix for real-time quantitative reverse transcription PCR (qRT-PCR) (PN:11752250 Life Technologies) according to manufacturer's protocols. qPCR was performed on a Bio-Rad CFX384 Real-Time PCR Detection System, with Kicqstart primer assays for *Mmp13, Il6, Tnf, Mmp3*, and *Gapdh* (KSPQ12012G, Sigma) in a final concentration of 10×10^{-6} M and SYBR Green qPCR Master Mix (PN:330513 Qiagen). Primer assay efficiencies were guaranteed by the manufacturer to be greater than 90%. Each reaction was measured using technical triplicates, and data were normalized to the expression levels of the housekeeping gene *Gapdh*. Results are presented as a fold-change compared to the average expression level in the untreated ankles using the ΔΔCq method.

Flow cytometry analysis

Anti-mouse antibodies against FoxP3 (PN: 11-5773-82, lot:2199652) and F4-80 (PN: 12-4801-80, lot: 2430442) were purchased from Invitrogen. Anti-mouse antibodies against CD4 (PN: 100428, Lot: B347337), CD45 (PN: 103130, lot: B349380), CD11b (PN: 101235, lot: B360998), CD11c (PN: 117346, lot: B325181), CD80 (PN: 104705, lot: B334893), CD86 (PN: 105115, lot: B315643), I-A/I-E (MHC2) (PN: 107628, lot: B350373), CTLA-4 (PN: 106309, lot: B357050), and Ly6G (PN: 127614, lot: B259670) were purchased from Biolegend. All cells were gated based on forward and side scatter characteristics to limit debris, including dead cells. The Zombie Aqua Fixable Viability Kit (Biolegend, lot:B333785) stain was used to separate live and dead cells. Antibodies were diluted 1:400. Gates were drawn based on fluorescence-minus-one controls, and the frequencies of positively stained cells for each marker were recorded. Intracellular/intranuclear stains were performed by first staining for surface markers according to manufacturer's protocols, then fixing and permeabilizing cells using the FoxP3 Fixation/Permeabilization Buffer Set (Invitrogen, 00-5523-00, lots:2333698, 2220750, 2203535). To quantify immune cell subsets in mouse ankles, ankles were harvested after sacrificing mice, skin was removed, and ankles were harvested and incubated at 37°C in a solution of Complete RPMI, 1 mg/mL Type VIII collagenase and 0.1 mg/mL DNAse I for 50 minutes with constant gentle agitation. The supernatant was filtered through a 70 μm cell strainer and subsequently stained for flow cytometry. To quantify immune cell subsets in the peripheral blood, red blood cells (RBC) were first lysed with RBC lysis buffer before proceeding with staining. Flow cytometry was performed using an Attune® NxT Acoustic Focusing cytometer analyzer (A24858) and data analyzed using FlowJo (BD) software.

Statistics

Sample sizes for animal studies were based on prior work with SKG and CIA mice without use of additional statistical estimations.[89,90] Results were analyzed where indicated using unpaired Student's *t*-test, one or two- way ANOVA, and Mann-Whitney rank test; each identified for each individual experiment in the figure legends. Data were analyzed using Graphpad Prism software.

Supplementary Material

Refer to Web version on PubMed Central for supplementary material.

Acknowledgments

The authors acknowledge technical assistance by the Joint Cell Isolation Core and the Joint Bioinformatics and Computational Core of the Microenvironment in Arthritis Resource Center (MARC) and the Biostatistics Unit of the Clinical and Translational Research Institute at UC San Diego. The authors acknowledge the use of facilities and instrumentation supported by NSF through the UC San Diego Materials Research Science and Engineering Center (UCSD MRSEC). Sequencing was performed at the La Jolla Institute for Immunology Next Generation Sequencing Core Facility RRID:SCR_023107.

Funding:

National Institutes of Health grant T32AR064194

National Institutes of Health grant F31AR079921 (DAM)

National Institutes of Health grant F31HL164055 (MDK)

National Institutes of Health grant P30AR073761 (NB)

National Institutes of Health grant R01AR081887 (NJS)

National Institutes of Health grant P30CA23100

National Institutes of Health grant UL1TR001442

National Science Foundation grant DMR-2011924

Arthritis National Research Foundation (NJS)

Hellman Fellowship (NJS)

Swedish Society for Medical Research (SSMF) grant S19-0062 (MNDS)

Foundation for Research in Rheumatology (MNDS)

IngaBritt och Arne Lundbergs Forskningsstiftelse (MNDS)

Sahlgrenska Academy, University of Gothenburg (MNDS)

The content is solely the responsibility of the authors and does not necessarily represent the official views of the funding agencies, which include the National Institutes of Health and the National Science Foundation.

References

(1). Fraenkel L; Bathon JM; England BR; St. Clair EW; Arayssi T; Carandang K; Deane KD; Genovese M; Huston KK; Kerr G 2021 American College of Rheumatology Guideline for the Treatment of Rheumatoid Arthritis. Arthritis & Rheumatology 2021, 73 (7), 1108–1123. [PubMed: 34101376]

(2). Smolen JS; Aletaha D Rheumatoid Arthritis Therapy Reappraisal: Strategies, Opportunities and Challenges. Nature Reviews Rheumatology 2015, 11 (5), 276–289. [PubMed: 25687177]

(3). Guo Q; Wang Y; Xu D; Nossent J; Pavlos NJ; Xu J Rheumatoid Arthritis: Pathological Mechanisms and Modern Pharmacologic Therapies. Bone Res 2018, 6, 15. 10.1038/s41413-018-0016-9. [PubMed: 29736302]

(4). Walsh DA; McWilliams DF Pain in Rheumatoid Arthritis. Current pain and headache reports 2012, 16 (6), 509–517. [PubMed: 23109051]

(5). Sarzi-Puttini P; Salaffi F; Di Franco M; Bazzichi L; Cassisi G; Casale R; Cazzola M; Stisi S; Battellino M; Atzeni F Pain in Rheumatoid Arthritis: A Critical Review. Reumatismo 2014, 66 (1), 18–27. [PubMed: 24938192]

(6). Prince FH; Bykerk VP; Shadick NA; Lu B; Cui J; Frits M; Iannaccone CK; Weinblatt ME; Solomon DH Sustained Rheumatoid Arthritis Remission Is Uncommon in Clinical Practice. Arthritis Research & Therapy 2012, 14 (2), R68. 10.1186/ar3785. [PubMed: 22429277]

(7). Jacquemin C; Molto A; Servy H; Sellam J; Foltz V; Gandjbakhch F; Hudry C; Mitrovic S; Granger B; Fautrel B Flares Assessed Weekly in Patients with Rheumatoid Arthritis or Axial Spondyloarthritis and Relationship with Physical Activity Measured Using a Connected Activity Tracker: A 3-Month Study. RMD open 2017, 3 (1), e000434. [PubMed: 28879046]

(8). Bykerk VP; Shadick N; Frits M; Bingham CO; Jeffery I; Iannaccone C; Weinblatt M; Solomon DH Flares in Rheumatoid Arthritis: Frequency and Management. A Report from the BRASS Registry. The Journal of Rheumatology 2014, 41 (2), 227–234. 10.3899/jrheum.121521. [PubMed: 24334643]

(9). Hewlett S; Sanderson T; May J; Alten R; Bingham III CO; Cross M; March L; Pohl C; Woodworth T; Bartlett SJ 'I'm Hurting, I Want to Kill Myself': Rheumatoid Arthritis Flare Is More than a High Joint Count—an International Patient Perspective on Flare Where Medical Help Is Sought. Rheumatology 2012, 51 (1), 69–76. [PubMed: 21565901]

(10). van Laar M; Pergolizzi JV Jr; Mellinghoff H-U; Merchante IM; Nalamachu S; O'Brien J; Perrot S; Raffa RB Pain Treatment in Arthritis-Related Pain: Beyond NSAIDs. The open rheumatology journal 2012, 6, 320. [PubMed: 23264838]

(11). Berthelot J-M; De Bandt M; Morel J; Benatig F; Constantin A; Gaudin P; Le Loet X; Maillefert J-F; Meyer O; Pham T A Tool to Identify Recent or Present Rheumatoid Arthritis Flare from Both Patient and Physician Perspectives: The 'FLARE'Instrument. Annals of the rheumatic diseases 2012, 71 (7), 1110–1116. [PubMed: 22072015]

(12). Nagy G; van Vollenhoven RF Sustained Biologic-Free and Drug-Free Remission in Rheumatoid Arthritis, Where Are We Now? Arthritis research & therapy 2015, 17 (1), 1–7. [PubMed: 25566937]

(13). Alivernini S; Peluso G; Fedele AL; Tolusso B; Gremese E; Ferraccioli G Tapering and Discontinuation of TNF-α Blockers without Disease Relapse Using Ultrasonography as a Tool to Identify Patients with Rheumatoid Arthritis in Clinical and Histological Remission. Arthritis research & therapy 2016, 18 (1), 1–7. [PubMed: 26732314]

(14). Baker KF; Skelton AJ; Lendrem DW; Scadeng A; Thompson B; Pratt AG; Isaacs JD Predicting Drug-Free Remission in Rheumatoid Arthritis: A Prospective Interventional Cohort Study. Journal of autoimmunity 2019, 105, 102298. [PubMed: 31280933]

(15). Alivernini S; MacDonald L; Elmesmari A; Finlay S; Tolusso B; Gigante MR; Petricca L; Di Mario C; Bui L; Perniola S; Attar M; Gessi M; Fedele AL; Chilaka S; Somma D; Sansom SN; Filer A; McSharry C; Millar NL; Kirschner K; Nerviani A; Lewis MJ; Pitzalis C; Clark AR; Ferraccioli G; Udalova I; Buckley CD; Gremese E; McInnes IB; Otto TD; Kurowska-Stolarska M Distinct Synovial Tissue Macrophage Subsets Regulate Inflammation and Remission in Rheumatoid Arthritis. Nature Medicine 2020, 26 (8), 1295–1306. 10.1038/s41591-020-0939-8.

(16). Chang MH; Levescot A; Nelson-Maney N; Blaustein RB; Winden KD; Morris A; Wactor A; Balu S; Grieshaber-Bouyer R; Wei K; Henderson LA; Iwakura Y; Clark RA; Rao DA; Fuhlbrigge RC; Nigrovic PA Arthritis Flares Mediated by Tissue-Resident Memory T Cells in the Joint. Cell Reports 2021, 37 (4), 109902. 10.1016/j.celrep.2021.109902. [PubMed: 34706228]

(17). Roberts WN; Daltroy LH; Anderson RJ Stability of Normal Joint Findings in Persistent Classic Rheumatoid Arthritis. Arthritis & Rheumatism: Official Journal of the American College of Rheumatology 1988, 31 (2), 267–271.

(18). Orange DE; Yao V; Sawicka K; Fak J; Frank MO; Parveen S; Blachere NE; Hale C; Zhang F; Raychaudhuri S RNA Identification of PRIME Cells Predicting Rheumatoid Arthritis Flares. New England Journal of Medicine 2020, 383 (3), 218–228. [PubMed: 32668112]

(19). Boissier M-C; Semerano L; Challal S; Saidenberg-Kermanac'h N; Falgarone G Rheumatoid Arthritis: From Autoimmunity to Synovitis and Joint Destruction. Journal of autoimmunity 2012, 39 (3), 222–228. [PubMed: 22704962]

(20). Lutzky V; Hannawi S; Thomas R Cells of the Synovium in Rheumatoid Arthritis. Dendritic Cells. Arthritis research & therapy 2007, 9 (4), 219. [PubMed: 17850683]

(21). Martin E; Capini C; Duggan E; Lutzky VP; Stumbles P; Pettit AR; O'Sullivan B; Thomas R Antigen-Specific Suppression of Established Arthritis in Mice by Dendritic Cells Deficient in NF-κB. Arthritis & Rheumatism 2007, 56 (7), 2255–2266. 10.1002/art.22655. [PubMed: 17599748]

(22). Wehr P; Purvis H; Law SC; Thomas R Dendritic Cells, T Cells and Their Interaction in Rheumatoid Arthritis. Clinical & Experimental Immunology 2019, 196 (1), 12–27. [PubMed: 30589082]

(23). Ueno H; Klechevsky E; Morita R; Aspord C; Cao T; Matsui T; Di Pucchio T; Connolly J; Fay JW; Pascual V Dendritic Cell Subsets in Health and Disease. Immunological reviews 2007, 219 (1), 118–142. [PubMed: 17850486]

(24). Banchereau J; Steinman RM Dendritic Cells and the Control of Immunity. Nature 1998, 392 (6673), 245–252. [PubMed: 9521319]

(25). Barrow M. An Overview of the NF-kB Mechanism of Pathophysiology in Rheumatoid Arthritis, Investigation of the NF-kB Ligand RANKL and Related Nutritional Interventions. Autoimmunity Reviews 2021, 20 (2), 102741. [PubMed: 33340772]

(26). Marok R; Winyard PG; Coumbe A; Kus ML; Gaffney K; Blades S; Mapp PI; Morris CJ; Blake DR; Kaltschmidt C Activation of the Transcription Factor Nuclear factor-κB in Human Inflamed Synovial Tissue. Arthritis & Rheumatism: Official Journal of the American College of Rheumatology 1996, 39 (4), 583–591.

(27). O'Sullivan BJ; Thomas R CD40 Ligation Conditions Dendritic Cell Antigen-Presenting Function through Sustained Activation of NF-κB. The Journal of Immunology 2002, 168 (11), 5491–5498. [PubMed: 12023343]

(28). Bozzalla-Cassione E; Grignaschi S; Xoxi B; Luvaro T; Greco MI; Mazzucchelli I; Bugatti S; Montecucco C; Manzo A Insights Into the Concept of Rheumatoid Arthritis Flare. Front Med (Lausanne) 2022, 9, 852220. 10.3389/fmed.2022.852220. [PubMed: 35372374]

(29). Page G; Lebecque S; Miossec P Anatomic Localization of Immature and Mature Dendritic Cells in an Ectopic Lymphoid Organ: Correlation with Selective Chemokine Expression in Rheumatoid Synovium. The Journal of Immunology 2002, 168 (10), 5333–5341. [PubMed: 11994492]

(30). Santiago-Schwarz F; Anand P; Liu S; Carsons SE Dendritic Cells (DCs) in Rheumatoid Arthritis (RA): Progenitor Cells and Soluble Factors Contained in RA Synovial Fluid Yield a Subset of Myeloid DCs That Preferentially Activate Th1 Inflammatory-Type Responses. The Journal of Immunology 2001, 167 (3), 1758–1768. [PubMed: 11466401]

(31). Khan S; Greenberg JD; Bhardwaj N Dendritic Cells as Targets for Therapy in Rheumatoid Arthritis. Nature Reviews Rheumatology 2009, 5 (10), 566–571. 10.1038/nrrheum.2009.185. [PubMed: 19798032]

(32). Zvaifler NJ; Steinman RM; Kaplan G; Lau LL; Rivelis M Identification of Immunostimulatory Dendritic Cells in the Synovial Effusions of Patients with Rheumatoid Arthritis. The Journal of clinical investigation 1985, 76 (2), 789–800. [PubMed: 3875632]

(33). Balanescu A; Radu E; Nat R; Regalia T; Bojinca V; Predescu V; Predeteanu D Co-stimulatory and Adhesion Molecules of Dendritic Cells in Rheumatoid Arthritis. Journal of cellular and molecular medicine 2002, 6 (3), 415–425. [PubMed: 12417058]

(34). Takemura S; Braun A; Crowson C; Kurtin PJ; Cofield RH; O'Fallon WM; Goronzy JJ; Weyand CM Lymphoid Neogenesis in Rheumatoid Synovitis. The Journal of Immunology 2001, 167 (2), 1072–1080. [PubMed: 11441118]

(35). Weyand CM; Goronzy JJ Ectopic Germinal Center Formation in Rheumatoid Synovitis. Annals of the New York Academy of Sciences 2003, 987 (1), 140–149. [PubMed: 12727633]

(36). McInnes IB; Schett G The Pathogenesis of Rheumatoid Arthritis. N Engl J Med 2011, 365 (23), 2205–2219. 10.1056/NEJMra1004965. [PubMed: 22150039]

(37). Benson RA; Patakas A; Conigliaro P; Rush CM; Garside P; McInnes IB; Brewer JM Identifying the Cells Breaching Self-Tolerance in Autoimmunity. The Journal of Immunology 2010, 184 (11), 6378–6385. 10.4049/jimmunol.0903951. [PubMed: 20421640]

(38). Page G; Miossec P Paired Synovium and Lymph Nodes from Rheumatoid Arthritis Patients Differ in Dendritic Cell and Chemokine Expression. The Journal of Pathology: A Journal of the Pathological Society of Great Britain and Ireland 2004, 204 (1), 28–38.

(39). Leung BP; Conacher M; Hunter D; McInnes IB; Liew FY; Brewer JM A Novel Dendritic Cell-Induced Model of Erosive Inflammatory Arthritis: Distinct Roles for Dendritic Cells in T Cell Activation and Induction of Local Inflammation1. The Journal of Immunology 2002, 169 (12), 7071–7077. 10.4049/jimmunol.169.12.7071. [PubMed: 12471143]

(40). Martin E; Capini C; Duggan E; Lutzky VP; Stumbles P; Pettit AR; O'Sullivan B; Thomas R Antigen-specific Suppression of Established Arthritis in Mice by Dendritic Cells Deficient in NF-κB. Arthritis & Rheumatism: Official Journal of the American College of Rheumatology 2007, 56 (7), 2255–2266.

(41). Capini C; Jaturanpinyo M; Chang H-I; Mutalik S; McNally A; Street S; Steptoe R; O'Sullivan B; Davies N; Thomas R Antigen-Specific Suppression of Inflammatory Arthritis Using Liposomes. The Journal of Immunology 2009, 182 (6), 3556–3565. [PubMed: 19265134]

(42). Ouaaz F; Arron J; Zheng Y; Choi Y; Beg AA Dendritic Cell Development and Survival Require Distinct NF-κB Subunits. Immunity 2002, 16 (2), 257–270. [PubMed: 11869686]

(43). Allen R; Chizari S; Ma JA; Raychaudhuri S; Lewis JS Combinatorial, Microparticle-Based Delivery of Immune Modulators Reprograms the Dendritic Cell Phenotype and Promotes

Remission of Collagen-Induced Arthritis in Mice. ACS Appl Bio Mater 2019, 2 (6), 2388–2404. 10.1021/acsabm.9b00092.

(44). Cifuentes-Rius A; Desai A; Yuen D; Johnston APR; Voelcker NH Inducing Immune Tolerance with Dendritic Cell-Targeting Nanomedicines. Nat. Nanotechnol 2021, 16 (1), 37–46. 10.1038/s41565-020-00810-2. [PubMed: 33349685]

(45). Hilkens CMU; Isaacs JD Tolerogenic Dendritic Cell Therapy for Rheumatoid Arthritis: Where Are We Now? Clinical & Experimental Immunology 2013, 172 (2), 148–157. [PubMed: 23574312]

(46). Benham H; Nel HJ; Law SC; Mehdi AM; Street S; Ramnoruth N; Pahau H; Lee BT; Ng J; Brunck ME Citrullinated Peptide Dendritic Cell Immunotherapy in HLA Risk Genotype–Positive Rheumatoid Arthritis Patients. Science translational medicine 2015, 7 (290), 290ra87–290ra87.

(47). van Laar JM Tolerogenic Dendritic Cell Therapy for Rheumatoid Arthritis (TOLERANT) ClinicalTrials.Gov Identifier: NCT05251870, 2022. https://clinicaltrials.gov/ct2/show/NCT05251870.

(48). Harry RA; Anderson AE; Isaacs JD; Hilkens CMU Generation and Characterisation of Therapeutic Tolerogenic Dendritic Cells for Rheumatoid Arthritis. Ann Rheum Dis 2010, 69 (11), 2042. 10.1136/ard.2009.126383. [PubMed: 20551157]

(49). Manolova V; Flace A; Bauer M; Schwarz K; Saudan P; Bachmann MF Nanoparticles Target Distinct Dendritic Cell Populations According to Their Size. European Journal of Immunology 2008, 38 (5), 1404–1413. 10.1002/eji.200737984. [PubMed: 18389478]

(50). Chen Y; Zhang J; Ge X; Du J; Deb DK; Li YC Vitamin D Receptor Inhibits Nuclear Factor κB Activation by Interacting with IκB Kinase β Protein*. Journal of Biological Chemistry 2013, 288 (27), 19450–19458. 10.1074/jbc.M113.467670. [PubMed: 23671281]

(51). Adorini L; Penna G; Giarratana N; Roncari A; Amuchastegui S; Daniel KC; Uskokovic M Dendritic Cells as Key Targets for Immunomodulation by Vitamin D Receptor Ligands. The Journal of Steroid Biochemistry and Molecular Biology 2004, 89–90, 437–441. 10.1016/j.jsbmb.2004.03.013.

(52). Lei C; Dongqing Z; Yeqing S; Oaks MK; Lishan C; Jianzhong J; Jie Q; Fang D; Ningli L; Xinghai H; DaMing R Association of the CTLA-4 Gene with Rheumatoid Arthritis in Chinese Han Population. Eur J Hum Genet 2005, 13 (7), 823–828. 10.1038/sj.ejhg.5201423. [PubMed: 15841095]

(53). Liu T; Lin X; Yu H Identifying Genes Related with Rheumatoid Arthritis via System Biology Analysis. Gene 2015, 571 (1), 97–106. 10.1016/j.gene.2015.06.058. [PubMed: 26117171]

(54). Hayer S; Vervoordeldonk MJ; Denis MC; Armaka M; Hoffmann M; Bäcklund J; Nandakumar KS; Niederreiter B; Geka C; Fischer A 'SMASH'Recommendations for Standardised Microscopic Arthritis Scoring of Histological Sections from Inflammatory Arthritis Animal Models. Annals of the rheumatic diseases 2021, 80 (6), 714–726. [PubMed: 33602797]

(55). Kaldybekov DB; Filippov SK; Radulescu A; Khutoryanskiy VV Maleimide-Functionalised PLGA-PEG Nanoparticles as Mucoadhesive Carriers for Intravesical Drug Delivery. European Journal of Pharmaceutics and Biopharmaceutics 2019, 143, 24–34. 10.1016/j.ejpb.2019.08.007. [PubMed: 31419584]

(56). Paka GD; Ramassamy C Optimization of Curcumin-Loaded PEG-PLGA Nanoparticles by GSH Functionalization: Investigation of the Internalization Pathway in Neuronal Cells. Mol. Pharmaceutics 2017, 14 (1), 93–106. 10.1021/acs.molpharmaceut.6b00738.

(57). Garizo AR; Castro F; Martins C; Almeida A; Dias TP; Fernardes F; Barrias CC; Bernardes N; Fialho AM; Sarmento B P28-Functionalized PLGA Nanoparticles Loaded with Gefitinib Reduce Tumor Burden and Metastases Formation on Lung Cancer. Journal of Controlled Release 2021, 337, 329–342. 10.1016/j.jconrel.2021.07.035. [PubMed: 34311024]

(58). Schmid D; Park CG; Hartl CA; Subedi N; Cartwright AN; Puerto RB; Zheng Y; Maiarana J; Freeman GJ; Wucherpfennig KW; Irvine DJ; Goldberg MS T Cell-Targeting Nanoparticles Focus Delivery of Immunotherapy to Improve Antitumor Immunity. Nat Commun 2017, 8 (1), 1747. 10.1038/s41467-017-01830-8. [PubMed: 29170511]

(59). Martínez-Jothar L; Doulkeridou S; Schiffelers RM; Sastre Torano J; Oliveira S; van Nostrum CF; Hennink WE Insights into Maleimide-Thiol Conjugation Chemistry: Conditions for Efficient

Surface Functionalization of Nanoparticles for Receptor Targeting. Journal of Controlled Release 2018, 282, 101–109. 10.1016/j.jconrel.2018.03.002. [PubMed: 29526739]

(60). Smyth DG; Nagamatsu A; Fruton JS Some Reactions of N-Ethylmaleimide1. J. Am. Chem. Soc 1960, 82 (17), 4600–4604. 10.1021/ja01502a039.

(61). Younes A; Bartlett NL; Leonard JP; Kennedy DA; Lynch CM; Sievers EL; Forero-Torres A Brentuximab Vedotin (SGN-35) for Relapsed CD30-Positive Lymphomas. New England Journal of Medicine 2010, 363 (19), 1812–1821. 10.1056/NEJMoa1002965. [PubMed: 21047225]

(62). Verma S; Miles D; Gianni L; Krop IE; Welslau M; Baselga J; Pegram M; Oh D-Y; Diéras V; Guardino E; Fang L; Lu MW; Olsen S; Blackwell K Trastuzumab Emtansine for HER2-Positive Advanced Breast Cancer. New England Journal of Medicine 2012, 367 (19), 1783–1791. 10.1056/NEJMoa1209124. [PubMed: 23020162]

(63). Sandborn WJ; Feagan BG; Stoinov S; Honiball PJ; Rutgeerts P; Mason D; Bloomfield R; Schreiber S Certolizumab Pegol for the Treatment of Crohn's Disease. New England Journal of Medicine 2007, 357 (3), 228–238. 10.1056/NEJMoa067594. [PubMed: 17634458]

(64). PubChem. Calcitriol. https://pubchem.ncbi.nlm.nih.gov/compound/5280453 (accessed 2023-05-28).

(65). Office of Dietary Supplements - Vitamin D. https://ods.od.nih.gov/factsheets/VitaminD-HealthProfessional/ (accessed 2023-05-28).

(66). He GZ; Lin WJ Peptide-Functionalized Nanoparticles-Encapsulated Cyclin-Dependent Kinases Inhibitor Seliciclib in Transferrin Receptor Overexpressed Cancer Cells. Nanomaterials 2021, 11 (3), 772. 10.3390/nano11030772. [PubMed: 33803751]

(67). Ramalho MJ; Loureiro JA; Gomes B; Frasco MF; Coelho MAN; Pereira MC PLGA Nanoparticles as a Platform for Vitamin D-Based Cancer Therapy. Beilstein J. Nanotechnol. 2015, 6 (1), 1306–1318. 10.3762/bjnano.6.135.

(68). Kim H-G; Gater DL; Kim Y-C Development of Transdermal Vitamin D3 (VD3) Delivery System Using Combinations of PLGA Nanoparticles and Microneedles. Drug Deliv. and Transl. Res 2018, 8 (1), 281–290. 10.1007/s13346-017-0460-x. [PubMed: 29247316]

(69). Almouazen E; Bourgeois S; Jordheim LP; Fessi H; Briançon S Nano-Encapsulation of Vitamin D3 Active Metabolites for Application in Chemotherapy: Formulation Study and in Vitro Evaluation. Pharm Res 2013, 30 (4), 1137–1146. 10.1007/s11095-012-0949-4. [PubMed: 23225028]

(70). Zhu GH; Gray ABC; Patra HK Nanomedicine: Controlling Nanoparticle Clearance for Translational Success. Trends in Pharmacological Sciences 2022, 43 (9), 709–711. 10.1016/j.tips.2022.05.001. [PubMed: 35659416]

(71). Adorini L. Tolerogenic Dendritic Cells Induced by Vitamin D Receptor Ligands Enhance Regulatory T Cells Inhibiting Autoimmune Diabetes. Annals of the New York Academy of Sciences 2003, 987 (1), 258–261. 10.1111/j.1749-6632.2003.tb06057.x. [PubMed: 12727648]

(72). Penna G; Amuchastegui S; Giarratana N; Daniel KC; Vulcano M; Sozzani S; Adorini L 1,25-Dihydroxyvitamin D3 Selectively Modulates Tolerogenic Properties in Myeloid but Not Plasmacytoid Dendritic Cells1. The Journal of Immunology 2007, 178 (1), 145–153. 10.4049/jimmunol.178.1.145. [PubMed: 17182549]

(73). Takeda M; Yamashita T; Sasaki N; Nakajima K; Kita T; Shinohara M; Ishida T; Hirata K Oral Administration of an Active Form of Vitamin D3 (Calcitriol) Decreases Atherosclerosis in Mice by Inducing Regulatory T Cells and Immature Dendritic Cells With Tolerogenic Functions. Arteriosclerosis, Thrombosis, and Vascular Biology 2010, 30 (12), 2495–2503. 10.1161/ATVBAHA.110.215459. [PubMed: 20930170]

(74). Rowshanravan B; Halliday N; Sansom DM CTLA-4: A Moving Target in Immunotherapy. Blood 2018, 131 (1), 58–67. 10.1182/blood-2017-06-741033. [PubMed: 29118008]

(75). Wang XB; Fan ZZ; Anton D; Vollenhoven AV; Ni ZH; Chen XF; Lefvert AK CTLA4 Is Expressed on Mature Dendritic Cells Derived from Human Monocytes and Influences Their Maturation and Antigen Presentation. BMC Immunol 2011, 12, 21. 10.1186/1471-2172-12-21. [PubMed: 21414236]

(76). Laurent S; Carrega P; Saverino D; Piccioli P; Camoriano M; Morabito A; Dozin B; Fontana V; Simone R; Mortara L; Mingari MC; Ferlazzo G; Pistillo MP CTLA-4 Is Expressed by Human

Monocyte—Derived Dendritic Cells and Regulates Their Functions. Human Immunology 2010, 71 (10), 934–941. 10.1016/j.humimm.2010.07.007. [PubMed: 20650297]

(77). Messemaker TC; Huizinga TW; Kurreeman F Immunogenetics of Rheumatoid Arthritis: Understanding Functional Implications. Journal of Autoimmunity 2015, 64, 74–81. 10.1016/j.jaut.2015.07.007. [PubMed: 26215034]

(78). Krüger JP; Endres M; Neumann K; Häupl T; Erggelet C; Kaps C Chondrogenic Differentiation of Human Subchondral Progenitor Cells Is Impaired by Rheumatoid Arthritis Synovial Fluid. Journal of Orthopaedic Research 2010, 28 (6), 819–827. 10.1002/jor.21058. [PubMed: 20041492]

(79). Malmström V; Bäcklund J; Jansson L; Kihlberg J; Holmdahl R T Cells That Are Naturally Tolerant to Cartilage-Derived Type II Collagen Are Involved in the Development of Collagen-Induced Arthritis. Arthritis Research & Therapy 2000, 2 (4), 315. 10.1186/ar106.

(80). Galea R; Nel HJ; Talekar M; Liu X; Ooi JD; Huynh M; Hadjigol S; Robson KJ; Ting YT; Cole S PD-L1–and Calcitriol-Dependent Liposomal Antigen-Specific Regulation of Systemic Inflammatory Autoimmune Disease. JCI insight 2019, 4 (18).

(81). Buzás EI; Végvári A; Murad YM; Finnegan A; Mikecz K; Glant TT T-Cell Recognition of Differentially Tolerated Epitopes of Cartilage Proteoglycan Aggrecan in Arthritis. Cellular Immunology 2005, 235 (2), 98–108. 10.1016/j.cellimm.2004.08.006. [PubMed: 16185673]

(82). Kimura A; Kishimoto T IL-6: Regulator of Treg/Th17 Balance. European Journal of Immunology 2010, 40 (7), 1830–1835. 10.1002/eji.201040391. [PubMed: 20583029]

(83). Jang D; Lee A-H; Shin H-Y; Song H-R; Park J-H; Kang T-B; Lee S-R; Yang S-H The Role of Tumor Necrosis Factor Alpha (TNF-α) in Autoimmune Disease and Current TNF-α Inhibitors in Therapeutics. International Journal of Molecular Sciences 2021, 22 (5), 2719. 10.3390/ijms22052719. [PubMed: 33800290]

(84). Burrage PS; Mix KS; Brinckerhoff CE Matrix Metalloproteinases: Role In Arthritis. FBL 2006, 11 (1), 529–543. 10.2741/1817.

(85). Bykerk VP; Shadick N; Frits M; Bingham CO; Jeffery I; Iannaccone C; Weinblatt M; Solomon DH Flares in Rheumatoid Arthritis: Frequency and Management. A Report from the BRASS Registry. The Journal of rheumatology 2014, 41 (2), 227–234. [PubMed: 24334643]

(86). Kim SH; Kim S; Evans CH; Ghivizzani SC; Oligino T; Robbins PD Effective Treatment of Established Murine Collagen-Induced Arthritis by Systemic Administration of Dendritic Cells Genetically Modified to Express IL-4. J Immunol 2001, 166 (5), 3499–3505. 10.4049/jimmunol.166.5.3499. [PubMed: 11207309]

(87). Kim SH; Kim S; Oligino TJ; Robbins PD Effective Treatment of Established Mouse Collagen-Induced Arthritis by Systemic Administration of Dendritic Cells Genetically Modified to Express FasL. Mol Ther 2002, 6 (5), 584–590. [PubMed: 12409256]

(88). Sonigra A; Nel HJ; Wehr P; Ramnoruth N; Patel S; van Schie KA; Bladen MW; Mehdi AM; Tesiram J; Talekar M Randomized Phase I Trial of Antigen-Specific Tolerizing Immunotherapy with Peptide/Calcitriol Liposomes in ACPA+ Rheumatoid Arthritis. JCI insight 2022, 7 (20).

(89). McBride DA; Kerr MD; Johnson WT; Nguyen A; Zoccheddu M; Yao M; Prideaux EB; Dorn NC; Wang W; Svensson MN; Bottini N; Shah NJ Immunomodulatory Microparticles Epigenetically Modulate T Cells and Systemically Ameliorate Autoimmune Arthritis. Advanced Science 2023, 2202720. [PubMed: 36890657]

(90). Svensson MN; Doody KM; Schmiedel BJ; Bhattacharyya S; Panwar B; Wiede F; Yang S; Santelli E; Wu DJ; Sacchetti C Reduced Expression of Phosphatase PTPN2 Promotes Pathogenic Conversion of Tregs in Autoimmunity. The Journal of Clinical Investigation 2019, 129 (3), 1193–1210. [PubMed: 30620725]

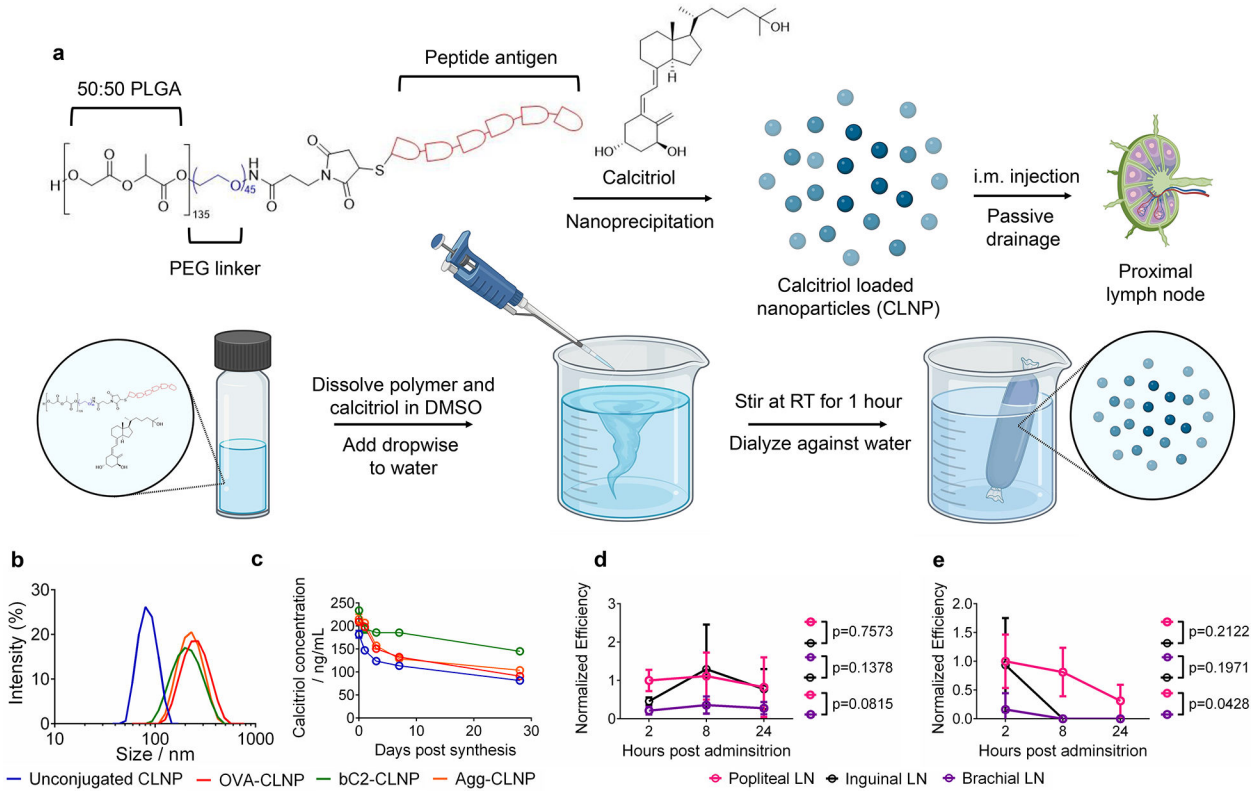

Figure 1.

Synthesis, characterization and biodistribution of CLNP formulations. (a) Experimental schematic and chemical structure of calcitriol loaded nanoparticle synthesis. (b) Dynamic light scattering by intensity graph of all four CLNP formulations. (c) Calcitriol concentration in all particle formulations in days post synthesis from storage conditions (DI water, 4°C), performed with three technical replicates. (d, e) Plots of Cy5 efficiency normalized to the 2-hour popliteal lymph node datapoint over 24 hours in inguinal, popliteal, and brachial lymph nodes; Cy5-PEG-PLGA in (d) and Cy5-Calcitriol in (e). Data is (c-e) are means ±SD of three experimental replicates. Statistical analyses in (d-e) were performed using two-way ANOVA. Schematic in (a) was composed using BioRender and ChemDraw.

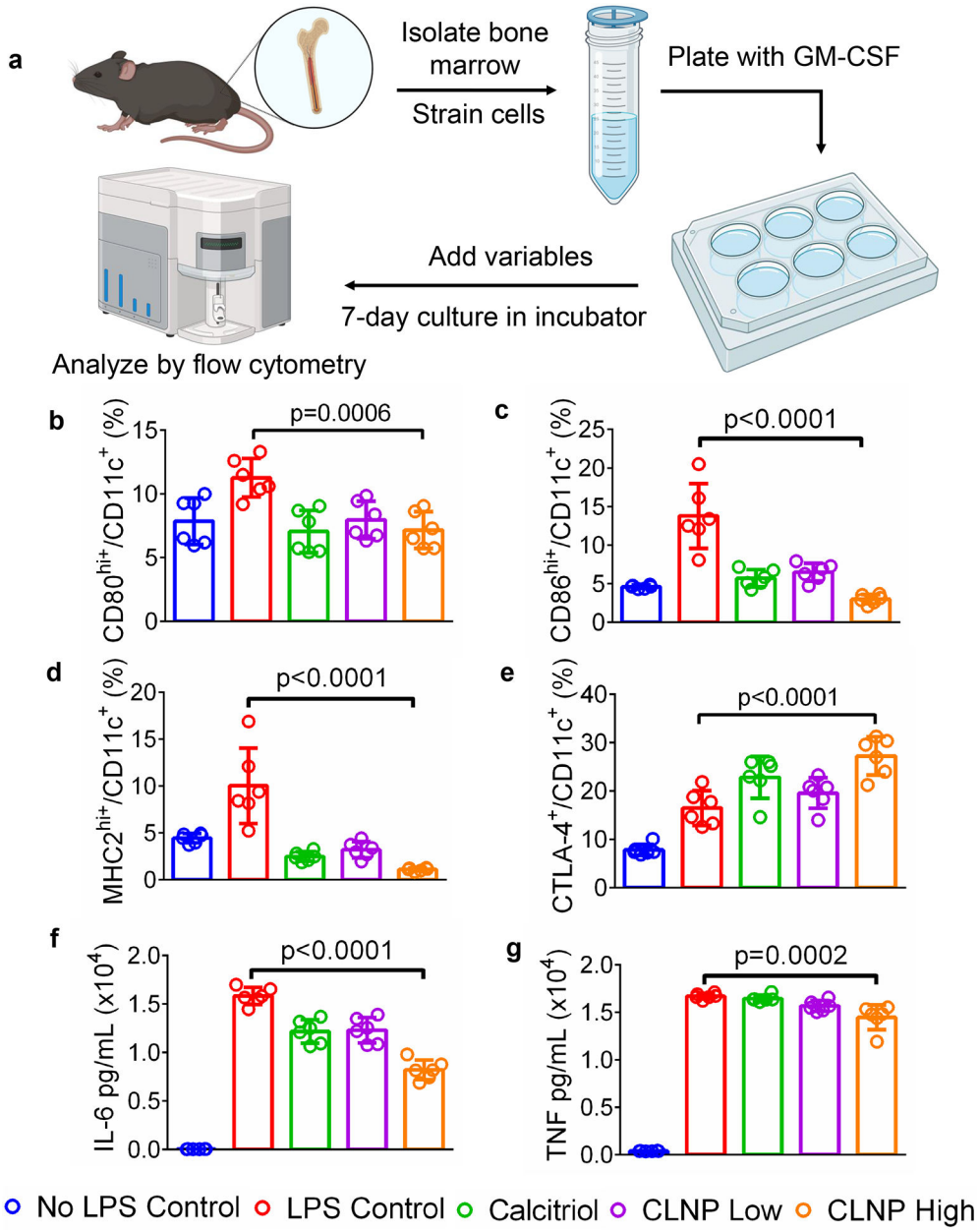

Figure 2.

CLNP imparts a tolerogenic phenotype on DC *in vitro*. (a) Experimental schematic of DC culutre. (b, c, d, and e) Costimulatory molecules (CD80 and CD86), major histocompatibility complex II (MHC2), and cytotoxic T-lymphocyte-associated protein 4 (CTLA-4) positivity on $CD11c^+$ DC after culture with/without LPS, free calcitriol, and two doses of CLNP as measured by (b) CD80, (c) CD86, (d) MHC2, and (e) CTLA-4. (f-g) Cytokine concentrations in DC media after culture with/without LPS, free calcitriol, and two doses of CLNP as measured by (f) IL-6 and (g) TNF. Data in (b-g) are means ±SD of six technical replicates from representative experiments. Statistical analyses in (b-g) were performed using ANOVA with Tukey's multiple comparison test. Schematic in (a) was composed using BioRender.

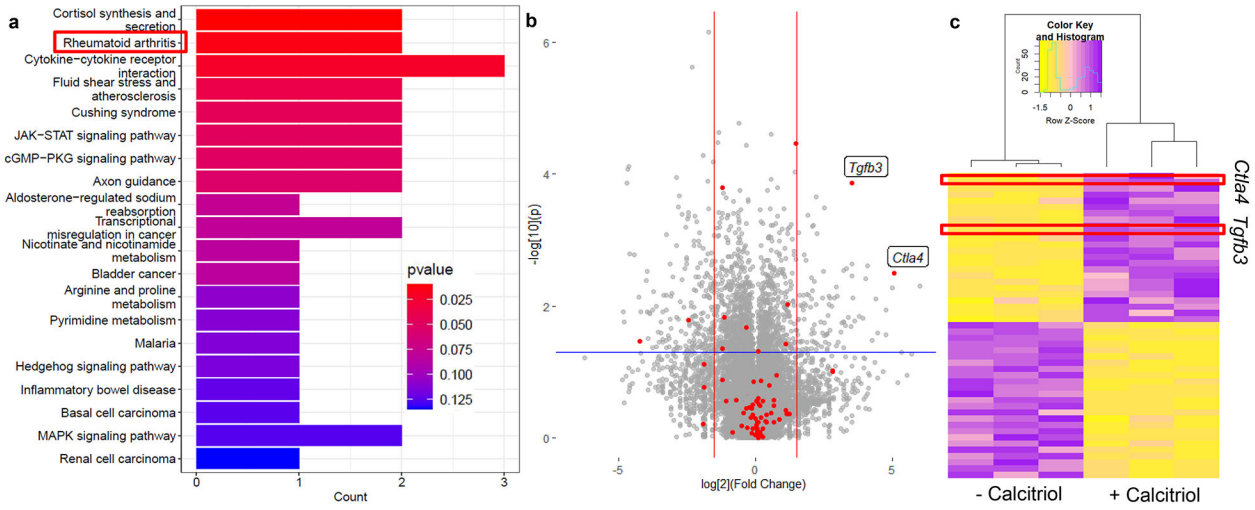

Figure 3.

Calcitriol modulates RA relevant targets in DC. (a) Pathway enrichment analysis based on top 50 DEG with RA boxed. (b) Volcano plot with RA-associated genes highlighted in red. (c) Heatmap and dendrogram comparing the top 50 DEG from bulk RNA-seq of −/+ Calcitriol DC, *Ctla4* and *Tgfb3* are highlighted. Data analyzed by quantile and TMM normalization. In (b), blue line represents a p value <0.05 and red lines indicate a fold change >1.5x by absolute value. In (c) each column represents a replicate of the respective condition and data represents the signal across each gene ranked as z-scores using data across each row.

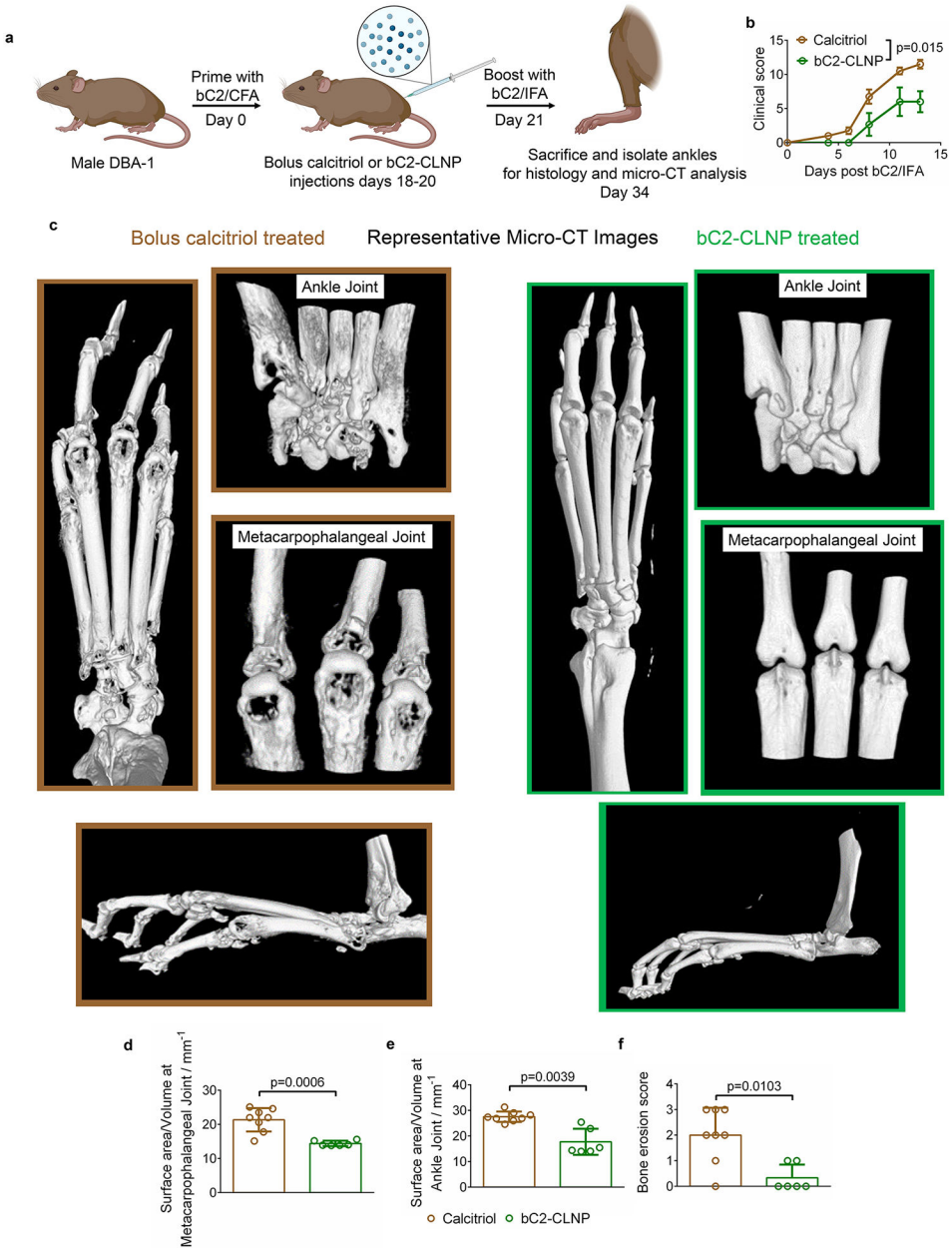

Figure 4.

bC2-CLNP reduce synovitis, cartilage destruction, and bone erosions in the CIA mouse model. (a) Schematic and timeline of experimental procedure. (b) Clinical scores of mice treated with either bolus calcitriol (10 ng calcitriol/biceps femoris/day, n=4) or bC2-CLNP (33 μg bC2-CLNP/biceps femoris/day, n=3). (c) Representative micro-CT images of hind paws from calcitriol and bC2-CLNP treated joints. Magnified images were used for treatment-blinded (d, e, f) bone surface area to volume quantification for the (d) metacarpophalangeal and (e) ankle joints as well as (f) bone erosion scoring. Statistical analyses were performed using (b) two-way ANOVA, (d-e) unpaired Student's *t*-test with Welsch's correction and (f) Mann-Whitney test. Schematic in (a) was composed using BioRender.

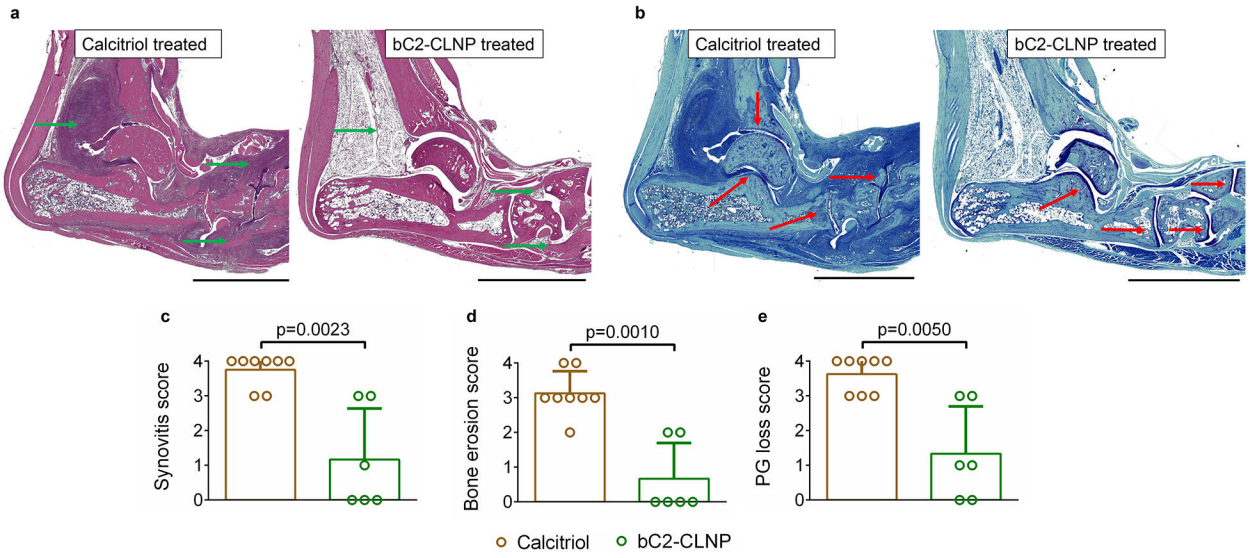

Figure 5.

Representative (a) H&E- and (b) toluidine blue-stained histological ankle sections from mice that received either calcitriol or bC2-CLNP depicting synovitis (green arrows) and proteoglycan loss (red arrows). Treatment-blinded (c) synovitis, (d) bone erosion and (e) proteoglycan loss scores from H&E- (c, d) and toluidine blue-stain (e) histological sections. Data in (c-e) represents means ±SD. Data (c-e) are from n=8 sections from 4 mice for the calcitriol group and n=6 sections from 3 mice for the bC2-CLNP group. Statistical analyses were performed using (c-e) Mann-Whitney test. Scale bar in (a, b) is 2 μm.

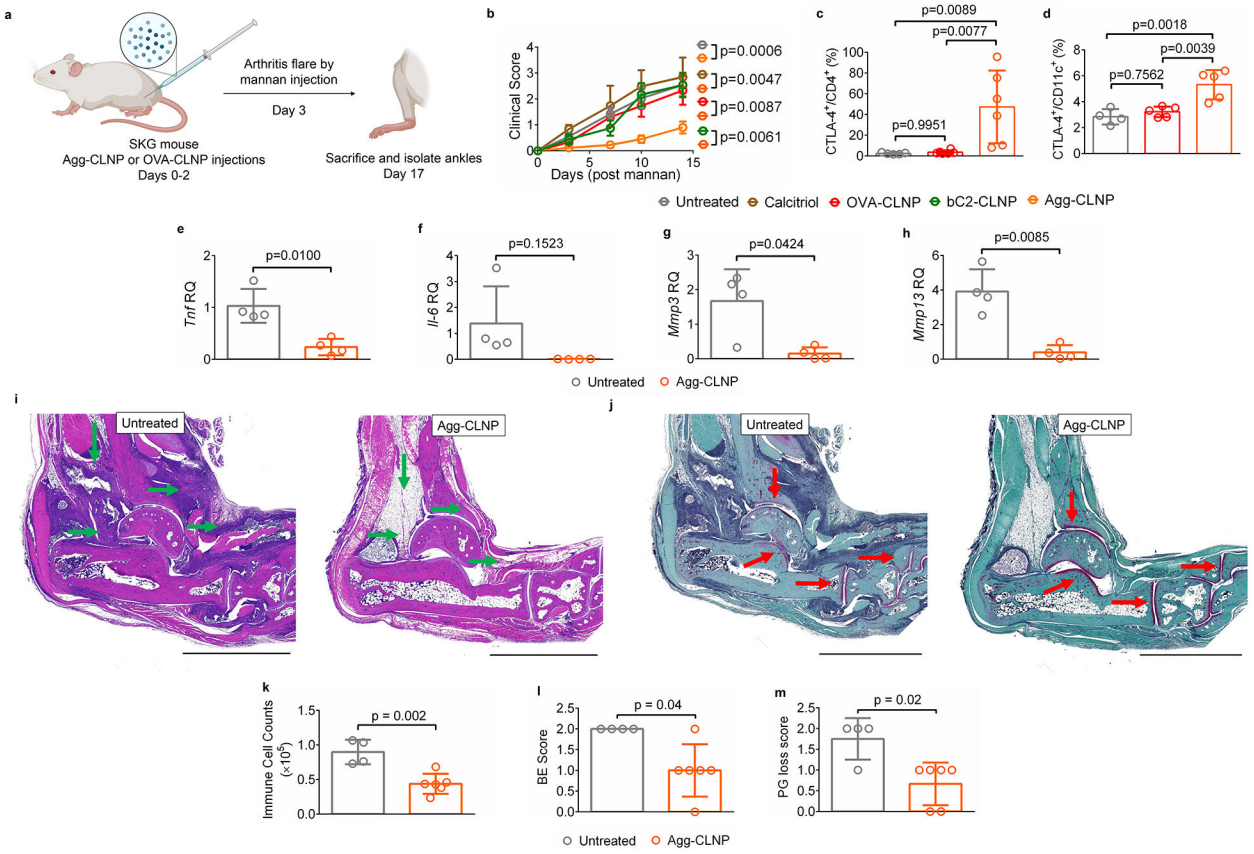

Figure 6.

Agg-CLNP modulate autoimmune arthritis in SKG mice. (a) Schematic and timeline of experimental procedure. (b) Clinical scores of mice with no treatment (untreated, n=5) and treated with bolus calcitriol (10 ng calcitriol/biceps femoris/day, n=4), OVA-CLNP (33 μg OVA-CLNP/biceps femoris/day, n=6), bC2-CLNP (33 μg bC2-CLNP/biceps femoris/day, n=6) or Agg-CLNP (33 μg Agg-CLNP/biceps femoris/day, n=6). (c) Quantification of CTLA-4^{+}CD4^{+} T cells isolated from the ankle fourteen-days post mannan. (d) Quantification of CTLA-4^{+} CD11c^{+} DC isolated from the ankle fourteen-days post mannan. qPCR relative quantification of (e) *Tnf*, (f) *Il6*, (g) *Mmp3*, and (h) *Mmp13*. Representative (i) H&E- and (j) safranin O-stained histological ankle sections from mice that received either no treatment or Agg-CLNP depicting synovitis (green arrows) and proteoglycan loss (red arrows). Treatment-blinded (k) synovitis, (l) bone erosion and (m) proteoglycan loss scores from H&E, H&E, and safranin O histological sections, respectively. Data in (b) represent means ±SEM and in (c-h, k-m) represent means ±SD. Data for immune cell counts, bone erosion and proteoglycan loss are from n=4 sections from 2 mice for the untreated group and n=6 sections from 3 mice for the Agg-CLNP group. Statistical analyses were performed using (b) two-way ANOVA, (c-h, k) unpaired Students *t*-test with Welsch's correction, and (l-m) Mann-Whitney test. Scale bar in (i, j) is 2 μm. Schematic in (a) was composed using BioRender.